Rock Bag Stability

Empirical research for the hydraulic stability of rock-filled mesh bags in offshore application for the stabilisation of cable protection systems

CIEM0500: MSc. Thesis

L.V. la Poutré

Delft University of Technology

TU Delft

Van Oord

Marine ingenuity

Rock Bag Stability

Empirical research for the hydraulic stability of rock-filled mesh bags in offshore application for the stabilisation of cable protection systems

by

L.V. la Poutré

in partial fulfilment of the requirements for the degree of

Master of Science
at the Delft University of Technology,

to be defended publicly on Thursday August 29, 2024 at 13:00 AM.

Student number: 4704770
Project duration: February 12, 2024 – August 29, 2024
Thesis committee: Dr. ir. Bas Hofland, TU Delft, supervisor
Dr. ir. Hayo Hendrikse, TU Delft, supervisor
Ir. Sagar Mungar, Van Oord
Ir. Robert Lengkeek, Van Oord

This thesis is under embargo and cannot be made public until August 29, 2025

Cover: Rock bags ready for deployment (Van Oord, 2024)

TU Delft

Van Oord
Marine ingenuity

Preface

This thesis was written as the final part of my master's degree in civil engineering at the Delft University of Technology. Over the past nine months I have had the pleasure of working with many amazing people and I would like to thank them for making this project possible.

First, I would like to thank my supervisors at Van Oord Sagar and Robert for giving me the opportunity to work on this project. Your encouragement and positive attitude were really motivating. You were always available to answer questions and provide feedback, which was very helpful and made my experience working on the project very nice. I also want to thank all my other colleges at Van Oord for their interest and advice throughout. You truly made me feel at home in Gorinchem.

I owe many thanks to my TU Delft supervisors. Bas, your enthusiastic and involved support helped me overcome many obstacles and introduced me to new ideas on how to solve the numerous problems we encountered. Without your feedback and brainstorming, the project would have been impossible. Hayo, thank you for your sharp questions and fresh perspectives that elevated the project.

I would like to thank the staff of the hydraulic engineering laboratory for their assistance throughout the project. Chantal, many thanks for all your help and for pushing me to specify my plans. Thank you, Pieter, for always being willing to help. Arno and Arie, your technical insights and practical skills enabled this project and allowed me to adapt to challenges that developed along the way.

Throughout this project and my previous years of study, my family has always been supportive. I am very grateful as without them I would not have been able to get to this point. Finally, Laurine, I want to thank you for always being there for me.

Lucas la Poutré
Rotterdam, August 2024

Summary

The expanding offshore wind industry is facing challenges with excessive movement of the power cables that connect offshore turbines to the grid. The casings that surround the exposed parts of cables near structures, known as cable protection systems (CPS), show damage before the end of their expected service life, requiring costly repair and maintenance. A potential solution is to stabilise the CPS by placing one or more rock-filled mesh bag (rock bag) on top of it. There are multiple rock bag manufacturers and distributors. The bags are made of polyester netting that is relatively flexible. The sizes considered for this study are 4 and 8 ton (4000 and 8000 kg), but smaller and larger sizes are available. Manufacturers recommend fill material with median diameters of 50 and 75 mm respectively. Currently, little is known about the behaviour and stability of these rock bags in offshore environments. The goal of this study is to expand the knowledge through empirical testing. The primary research question is: *What is the hydraulic stability of rock bags under wave loading in offshore application for the stabilisation of CPS?*

To answer this question, 480 experiments were conducted in a flume, measuring 36 metres in length by 0.9 metres high and 0.76 metres wide, in the hydraulic engineering laboratory of Delft University of Technology. Two set-ups were used, one with a flat rough bed, to test two or three rock bags side by side and grouped formations of bags. The other is a realistic halved model of a monopile, scour protection and CPS. Regular wave, irregular wave and combined wave-current conditions have been tested. The scales used in the experiments are 1:40 and 1:30. Two scales are used to be able to detect possible scaling effects. Scaling is principally done according to Froude's law. A single monopile and CPS are used for both scales, which represent different prototype sizes. The rough bed and scour protection used are made of glued rocks.

The Froude scaling is adjusted for the fill material size, to account for differences in critical mobility and density between model and prototype fill materials. To compensate for the difference in permeability of the fill material between prototype and model scales, narrow-graded fill material is used to increase porosity. Two bags are included with wide-graded fill material to determine the influence of the porosity of fill material. The mesh material used for the model bags is tulle, which attempts to represent the flexible prototype mesh. As the internal friction of the fill material might lead to the model bags moving too much as a rigid body with smaller deformations as a result, several tests with glass spheres as fill material are performed. In this way, a limit case for very low internal friction is made to be able to determine the influence of a very deformable bag.

Due to the large influence of reflections for the high regular waves, an analysis method is developed to account for the influence of these reflections on near bed orbital velocity. The orbital velocity for the incoming wave is determined by fitting the 5th-order Stokes wave to the leading waves of the measurement. The reflection was determined by subtracting this signal from the total wave signal. Next, the spatial and temporal interference pattern of the final standing wave can be reconstructed. This method was compared with velocity measurements that were performed at two locations between the set-up and wave gauges. For the tests with increased constructive interference at the set-up, the increased velocities were taken into account in the analysis. For the others the largest velocities of the leading waves are used.

Analysis of before and after top images of the tests is used to establish a failure criterion. Bags that are displaced by more than 1/6th of their diameter, approximately equal to a CPS diameter, are classified as failed; those with less displacement classified as rocking; and with only local changes of the shape or no differences are classified as stable. This corresponds to the four levels of movement observed during the flat bed tests. These are: local internal material movement, partial bag uplift, rocking of the entire bag, and overturning.

The test results are compared to the empirical stability limit defined by Jacobsen et al. (2023). They found a dependence of the stability on the ratio of inertia-drag forces expressed by the Keulegan-Carpenter number $KC = uT/D_{rb}$. Where u is the amplitude of wave orbital velocity, T is the period of the osculation and Drb is the diameter of the rock bag. From their results, the limit could be defined up to $KC = 15$, but they hypothesised an extended limit for larger values, where the limit is constant. Using the newly defined failure criterion, the results of the present study validate this extended limit as a lower bound for the occurrence of failure in regular waves for $KC < 25$.
Based on the results, a comparison can be made between the stability in regular and irregular wave fields. When orbital velocities are calculated with linear wave theory from the 2% exceedance probability wave height $u_{2\%LWT}$ and the peak period T_p, the stability limit seems to be a good predictor for the occurrence of failure.

In regular wave tests, the bags filled with glass spheres were considerably less stable. Therefore, internal friction is a relevant parameter that should be considered in physical model studies and designs based on the outcome these studies. It is suggested to include a factor in the stability limit to account for the uncertainty about the scale effect of internal friction. With a minimum value equal to the difference between the stability limit of low friction glass fill material and rock fill: $0.75 \leq K_{fr} \leq 1$.
The size of fill material was varied in regular wave tests this did not result in large differences in stability for the tested range. For irregular waves, there was a difference. In conditions that exceeded the stability limit, bags that were filled with larger material were more likely to fail. This is unexpected, as larger materials are generally expected to be less mobile.
Two bags were also made with wide-graded fill material to determine the effect of the narrow-graded fill material. In regular wave tests there was little difference. In irregular wave tests the wide-graded fill material bags were less likely to fail above the limit compared to the large fill material bags. There were slight differences with the small narrow-graded material as well. Thus, it is recommended to use narrow-graded fill material in further model tests, as these represent the porous flow mechanism much better.

For grouped bags, the four bag diamond formation performed best. It is considerably more stable compared to a single bag in the flat bed and full model set-up. An increase in stability of up to 1.5 was observed. This can be represented in the stability equation by a factor of $1 \leq K_g \leq 1.5$.
For the tested conditions, the addition of a steady current with magnitudes of up to 45% of the 2% exceedance probability orbital velocity amplitude, did not alter the stability of the rock bags.
Bags placed close to a monopile for CPS stabilisation have a decrease in stability. This decrease is proportional to the expected level of flow amplification near a monopile based on potential flow and turbulence. The CPS appears to effect the failure mechanism by applying force to the bag. The loss of stability can be accounted for with a factor in the stability equation K_v:

$$K_v = \begin{cases} 1 & \text{if } KC < 8.2 \\ \sqrt{0.122 \cdot KC} & \text{if } 8.2 \leq KC < 15 \\ 1.35 & \text{if } KC \geq 15 \end{cases} \tag{1}$$

The answer to the main question can be summarized in the following way: The extended Jacobsen et al. (2023) limit can be used to describe the stability of rock bags. This limit is based on the orbital velocity calculated from linear wave theory using the 2% wave height and peak period. Flow amplification, grouping and loads transferred by the CPS need to be considered. The stability limit:

$$\frac{(K_v u_{2\%})^2}{(s-1)gD_{rb}} < K_g K_{fr} \psi_{cr}, \quad \psi_{cr} = \begin{cases} 0.04 & \text{if } KC < 2.67 \\ 0.015 \cdot KC & \text{if } 2.67 \leq KC < 15 \\ 0.225 & \text{if } 15 \leq KC \leq 25 \end{cases} \tag{2}$$

For $KC = \frac{u_{2\%}T_p}{D_{rb}}$, with T_p the peak period, D_{rb} the diameter of the rock bag and the ratio of rock and water densities $s = \frac{\rho_s}{\rho_w}$. Due to the limited number of combined grouped formation tests with the monopile and CPS the combined use of the grouping factor K_g and the flow amplification factor K_v carries considerable uncertainty.

Nomenclature

Abbreviations

Abbreviation	Definition
Rock Bag	A rock-filled mesh bag; also known as rock net and filter unit (FU)
CPS	Cable protection system
EMS	Electromagnetic flow velocity sensor
ARC	Active reflection compensation
LWT	Linear wave theory
JONSWAP	Joint North Sea Wave Observation Project (Hasselmann et al. 1973)

Symbols

Symbol	Definition	Unit
H_{rb}	Height of the rock bag; height of the top of the rock layer	$[m]$
D_{rb}	Diameter of the of part of the rock bag in contact with the bed	$[m]$
F_{lift}	Hydrodynamic lift force	$[N]$
F_{drag}	Hydrodynamic drag force	$[N]$
$F_{internal}$	Internal friction force	$[N]$
W_{rb}	Effective self weight of the rock bag	$[N]$
Re	Reynolds number $Re = ul/\nu$	[-]
KC	Keulegan-Carpenter number $KC = uT/D$	[-]
u	Velocity in the x direction	$[m/s]$
l	Characteristic length	$[m]$
ρ_w	Density of water	$[kg/m^3]$
ρ_{rock}	Density of rock	$[kg/m^3]$
s	Effective density $= \rho_{rock}/\rho_w$	[-]
A_{rb}	Frontal area rock bag	$[m^2]$
V_{rb}	Volume rock bag	$[m^3]$
d_{50}	The diameter exceeded by 50% of the material measured by mass	$[m]$
k_s	Characteristic grain roughness	$[m]$
C_{lift}	Coefficient of lift	[-]
C_{drag}	Coefficient of drag	[-]
C_m	Coefficient of added mass	[-]
ψ_{cr}	Critical stability parameter	[-]
g	Gravitational acceleration $= 9.81$	$[m/s^2]$
T	Oscillation period	[s]
I	Hydrodynamic pressure gradient	[-]
u_{filter}	Filter velocity in porous granular material	$[m/s]$
a	Laminar flow drag coefficient	$[s/m]$
b	Turbulent flow drag coefficient	$[s^2/m^2]$
α	Laminar flow material drag coefficient	[-]

Symbol	Definition	Unit
β	Turbulent flow material drag coefficient	[-]
n	Porosity	[-]
KC_p	Keulegan-Carpenter number of porous flow $KC_p = \frac{u_{filter}T}{nd_{50}}$	[-]
H	Wave height	$[m]$
T	Wave period	$[s]$
L	Wave length	$[m]$
k	Wave number, defined as $\frac{2\pi}{L}$	$[rad/m]$
d	Water depth	$[m]$
H_{m0}	Significant wave height	$[m]$
Tp	peak wave period	$[s]$
$H_{2\%}$	2% Exceedance probability wave height	$[m]$
D_{pile}	Diameter of monopile	$[m]$
KC_{pile}	Keulegan-Carpenter number of near monopile flow $KC = uT/D_{pile}$	[-]
K_v	Flow amplification factor	[-]
K_g	Grouping factor	[-]
K_{fr}	Internal friction uncertainty factor	[-]

Contents

1

Introduction

1.1. Context

In the global energy transition, offshore wind energy will play an important role. Recent initiatives such as the European Green Deal, by the European Union and its member states, are massively speeding up investment in renewable energy, such as offshore wind (The North Seas Energy Cooperation, n.d.). For example, the Netherlands aims to achieve 21 gigawatts of offshore wind capacity by 2031, up from 2.5 gigawatts in 2023 (RVO, n.d.).

To transmit these gigawatts onshore, subsea power cables connect each turbine to offshore high voltage stations within the wind parks. The energy is then transported to the onshore users. Close to the structure, the cable is exposed as it exits the monopile and runs over the scour protection before being buried in the seabed. To prevent excessive loads in the cable during installation a casing is used that remains around the cable post installation. These casings are called Cable Protection Systems (CPS). They can have a diameter of up to half a metre (Topsector Energie Projecten, n.d.).

Figure 1.1: A rock bag is deployed near a monopile foundation (Ridgeway, 2024)

At the moment the wind energy industry is facing challenges with these systems. As many CPS' show significant damage well before reaching the end of their intended service life (Tramontanaengineering, n.d.). The costs associated with repairing the damaged CPS and cables can be substantial (Durakovic and Offshorewind.biz, 2022). Expansion into higher-energy areas will result in increased loads, so stabilisation may become required for the structural strength of the CPS.

The wear on these systems indicates that the present design does not appear sufficient and measures need to be taken to stabilise and protect the cables. One proposed solution is to stabilise the CPS by placing a rock-filled mesh bag (rock bag) on exposed sections as cover. Damage to CPS' is mostly seen in wind farms where no cover was placed. This suggests stabilisation has a beneficial impact on overall performance of the CPS (Topsector Energie Projecten, n.d.).

1.2. Problem and scope

The challenge when applying these rock bags is that there are no adequate design rules or equations for hydraulic stability in offshore conditions, nor for the combination with a CPS and monopile. As a result, an iterative design approach must be used, with empirical testing necessary for each situation. This is a costly and time-consuming process. This project aims to expand the knowledge of hydraulic stability for rock bags in various conditions given the following constraints:

- As the aim of the research is to expand the knowledge on rock bags, no comparison to other methods for CPS stabilisation is made. Stabilisation of the CPS with one or more rock bags is assumed to be effective in preventing damage. The effect of the remaining stresses in the CPS or cable is not considered;
- The research is focused on bags of flexible mesh material filled with relatively small granular material;
- The types considered are 4 and 8 tonnes rock-filled mesh bags, with diameters of 2.4 and 3 meters based on the manufacturer's specifications (Ridgeway, 2024, Bluemont, 2024 and Cirtex, 2023);
- The strength, integrity or durability of the bag material itself is not investigated and the filling material is not allowed to escape the bag;
- Only stability near monopile foundations is evaluated, as these account for 80% of the market share (Gupta and Basu, 2020). Monopile foundations with a diameter of 7.5-10 meters are considered;
- Monopiles are generally used in water depths from 20-40 metres. At these depths a scour protection is needed;
- Because rock bags are typically placed on the amour layer of the scour protection around a monopile, this research focuses stability on rough beds, so no tests for smooth beds are performed;
- Research from design studies indicates that the critical conditions for rock bag and CPS combinations occur when rock bags are positioned on the side of the monopile relative to the wave direction. So, these are the angles considered for this study;
- The hydraulic conditions considered for this study are wave dominated conditions, with wave fields based on North Sea waves;

1.3. Research questions

The aim of this project is to determine the hydraulic stability of rock bags in offshore conditions, with a focus on the loading due to waves and the stabilisation of cps's near monopile wind turbines. The objective is to derive a stability relation and validate the parameters. The empirically found relation can be used to determine the required dimensions of rock bags in early design stages. The main research question for this project is:*What is the hydraulic stability of rock bags under wave loading in offshore application for the stabilisation of CPS.* The answer to this question will be built up with the following sub-questions:

1. How do rock bags respond in offshore wave loading, what are the observed motions and failure mechanisms?
2. Which properties of rock bags influence stability, and how can their influence be quantified?
3. What is the limit for stability that can be derived from the experiments, and how does this compare to the literature?
4. What is the stability in an irregular wave field, and which wave statistic most accurately quantifies it?
5. What is the influence of grouping or stacking multiple rock bags on stability, considering formations applicable to CPS stabilization?
6. What is the stability of rock bags when applied in a CPS stabilization application near a monopile foundation and what is their performance in stabilizing the CPS?

.

1.4. Approach

To answer the questions, a two-pronged approach is chosen. A theoretical framework is constructed based on a literature study and analysis of the underlying mechanisms for rock bag mobility. The goal of this part of the study is to find a relation that can be used to express the stability of rock bags. This relation contains a number of unknown values that have to be filled in.
The second part of the research consists of physical model testing. These tests are done to be able to fill in the unknowns in the constructed equation. Because many tests are needed in a controlled environment, laboratory model tests are the best approach. The drawback of this method is the need to scale from prototype to model scale. Since there is very little data available at the moment and the failure mechanism of rock bags is uncertain, numerical models are not feasible as those have to be calibrated.

2

Theoretical framework

This chapter provides three theoretical analyses of the processes that govern the stability of one or more rock bags. The mechanisms of mobility are discussed in two parts in the first section, based first on the mechanisms mentioned in literature and then on a further analysis of stability.
The next section discusses the impact of rock bag porosity. This is based on literature on porous flow in large granular materials, such as those used to fill rock bags.
The final section discusses how a monopile influences the surrounding flow. This has the potential to significantly impact the stability of rock bags and CPS in the zone of influence.

2.1. Mechanisms of mobility for rock bags

In literature, a number of mobility mechanisms for rock bags are described for different bed types and configurations. An overview is presented in table 2.1.
Instantaneous displacement is likely to occur due to the lift force exceeding the weight of the rock bag, possibly due to turbulent vortexes in the vicinity of a structure. This was described for a rock bag scour protection around a monopile. For a single rock bag or small formation an overturning mechanism should be more critical due to the added drag force on the frontal area of the rock bag. In a rock bag scour protection the bags are shielded by each other reducing this drag force. On the edges of the scour protection the overturning mechanism is predicted to be be critical (Riezebos et al., 2021). This mechanism is shown in figure 2.1.
In this study a rough fixed bed is considered, hence failure mechanisms associated with other bed types are out of scope of this study and not considered. This includes sliding and undermining of rock bags.

Mobility mechanism	Jacobsen et al., 2023	Riezebos et al., 2021	Bed type	Responsible process
Instantaneous displacement		x	Rough	Lift, turbulence
Reshaping		x	Rough	Drag, internal mobility
Rocking / Rolling	x	x	Rough	Drag, lift, turbulence
Sliding	x		Smooth	Drag, lift
Undermining of rock bag		x	Active reshaping	Drag, reshaping bed

Table 2.1: Failure mechanisms of rock bags as described in two works of literature, along with the type of bed on which the bags were placed and the process suspected to be responsible.

For the rocking, rolling and reshaping failure mechanisms the overturning moment by various hydraulic forces is important. By assuming the rock bag as a rigid body a moment balance can be made for overturning around the rear end of the rock bag. In figure 2.1 the free body diagram is shown. Jacobsen et al. (2023) developed an Izbash type stability equation based on the moment balance of the lift force F_{lift}, drag force F_{drag} and weight of the rock bag W_{rb}:

$$F_{lift}\frac{D}{2} + F_{drag}\frac{H_{rb}}{2} = W_{rb}\frac{D}{2} \tag{2.1}$$

The drag force is determined by the ratio of inertial and viscous forces described by the Reynolds number $Re = ul/\nu$. With u the flow velocity, ν the kinematic viscosity and the characteristic length is equal to the diameter for rock bags $l = D_{rb}$. For rock bags to fail, substantial flow velocities are required, so the flow regime will be turbulent $Re > O(10^3)$. In turbulent flows the skin drag becomes negligible and the drag force can be defined as (Hofland, 2005):

$$F_{drag} = \frac{1}{2} C_{drag} \rho_w A_{rb} u^2 \tag{2.2}$$

Velocity differences over the rock bag can result in a lift force, defined as (Hofland, 2005):

$$F_{lift} = \frac{1}{2} C_{lift} \rho_w A_{rb} u^2 \tag{2.3}$$

The moment balance can now be rewritten to:

$$\frac{1}{2} C_{lift} \rho_w A_{rb} u^2 \frac{D}{2} + \frac{1}{2} C_{drag} \rho_w A_{rb} u^2 \frac{H_{rb}}{2} = W_{rockbag} \frac{D}{2} \tag{2.4}$$

$$W_{rockbag} = (\rho_{rock} - \rho_w) V_{rock} g \tag{2.5}$$

The diameter can be defined as a shape parameter α multiplied by the ratio of rock volume V_{rock} and frontal surface area A_{rb}:

$$D = \alpha \frac{V_{rock}}{A_{rb}} \tag{2.6}$$

The equation can be rewritten, with the ratio of rock and water densities $s = \frac{\rho_{rock}}{\rho_w}$:

$$\frac{u^2}{(s-1)gD} = \frac{2\alpha}{C_{drag} H_{rb}/D + C_{lift}} = \psi_{cr} \tag{2.7}$$

Since the right hand side of equation 2.7 only contains constants it can be expressed with a single empirical value ψ_{cr}. The ratio of height over diameter and α can differ between different types of rock bag. Since this difference is small it is not taken in to account (four ton bag $H/D = 0.25$, eight ton bag $H/D = 0.233$).

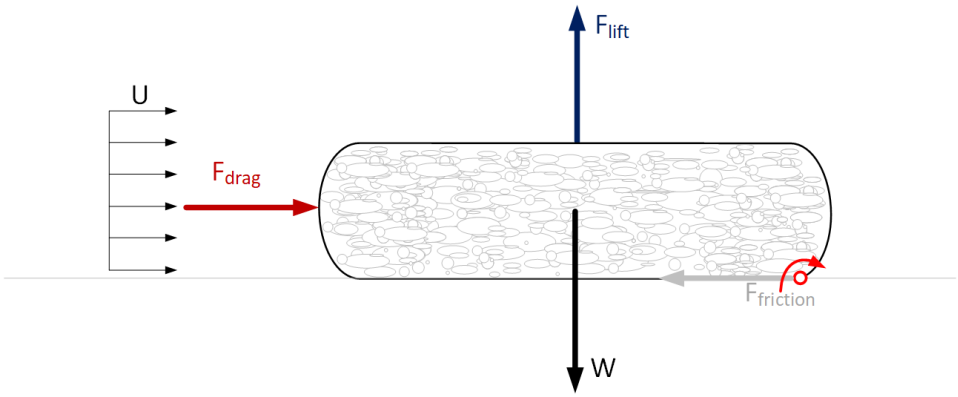

Figure 2.1: Free body diagram of rigid body overturning mechanism

The presented definition for the stability number lacks an inertia force term. The accelerating mass of water in oscillatory flow causes a force on the rock bag, whose magnitude is determined by the added mass coefficient C_m. The pressure gradient also applies a force on the rock bag, so the force consists of two parts (Hofland, 2005, Maxey and Riley, 1983). Due to the dependence on the acceleration $\frac{\partial u}{\partial t}$ the inclusion of such a term adds complexity to the definition. The inertia force for a stable rock bag can be written as:

$$F_{inertia} = (1 + C_M) \rho_w V \frac{\partial u}{\partial t} \tag{2.8}$$

Because of the lack of an inertia term in the equation Jacobsen et al. (2023) found the stability limit depends on the Keulegan–Carpenter (KC) number (eq. 2.9). This describes the ratio of drag to inertial forces on an object. For larger KC, with higher relative importance of drag force, the stability increases.

$$KC = \frac{U_{wave} * T}{D_{rb}} \tag{2.9}$$

Jacobsen et al. (2023) defined the limit based on experiments in the range $0 < KC < 15$. It was hypothesised that as KC further increased, the dependence of stability on KC is lost. So ψ_{cr} is constant for $KC > 15$.
In their experimental campaign they also found a similarly defined limit for stability in steady currents, that could be described as a limit for $KC \to \infty$. This empirical value is larger compared to the maximum value found for waves, indicating a major influence of the inertia force.

Contrary to what is suggested by Jacobsen et al. (2023), the limit cannot be applied for wave-current conditions. Adding the current velocity to the wave velocity amplitude would include it in the magnitude of inertial forces assumed in the empirical value. Since steady current has no acceleration, such a summation would diminish the physical basis of the limit.
For the assessment of loose rock bed protection in combined wave and current conditions, the addition of shear stresses in Shields type mobility numbers is commonly used (Soulsby, 1997, Van Rijn, 2019, Vos et al., 2011). A friction factor is calculated for both wave and current velocity (Dixen et al., 2008, Roulund et al., 2016). The factors are based on the material's characteristic grain roughness, which is commonly defined as $k_s = 2.5 * d_{50}$ for a layer of loose rock. Because rock bags are solitary elements that protrude above the bed level, the friction factors could be different. The magnitude of these factors must be determined through empirical research.

In this research the Jacobsen et al. (2023) stability equation is used due to its simplicity and inclusion of only one empirical constant. In the next section the applicability of this equation for more realistic non-rigid mobility is discussed.

2.1.1. Analysis of non-rigid mobility

The rigid body assumption is unrealistic because rock bags reshape under loading. As a result, a non-rigid failure analysis is conducted. The analysis is based on the observation of a portion of the bag being lifted. This is possible because the bag is flexible. Such partial lift can occur at lower drag and lift forces.

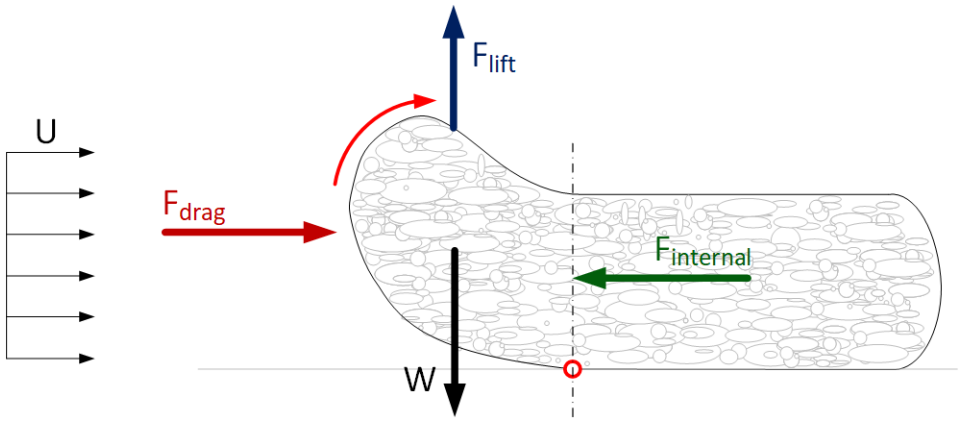

Figure 2.2: Free body diagram of realistic non-rigid partial uplift mechanism

Figure 2.2 shows a more realistic movement of the rock bag based on the mechanism described in the present study, see section 5.1. As the same balance of forces is responsible for the movement, this will be taken into account in the empirical value. When a large enough part of the bag is lifted in this manner the added frontal surface area and inertia of the moving part of the bag will cause complete overturning failure of the bag. Internal friction of the fill material is thought to have an influence on this

failure mechanism. The internal friction determines the rigidity of the bag. This is schematised as a counteracting force against the partial overturning of the bag $F_{internal}$. Thus, it is reasonable to apply the Jacobsen et al. (2023) limit to bags which fail in a non-rigid manner.

2.1.2. Influence of additional parameters on stability

In theory, smaller material has a higher mobility. In hydraulic conditions exceeding stability, the transport rate of smaller material will also be greater. This suggests a possible influence of the size of fill material on the stability of the rock bag.
More complex environments are also tested in this study, such as grouped bag formations and CPS stabilisation near a monopile. Shielding and turbulence create more complicated hydraulic forces in these grouped formations. A diagram of rock bags in a formation can be seen in figure 2.3. In grouped formations, the support of other bags can provide a counteracting force. The CPS can apply force on the rock bag F_{CPS} ,as can be seen in figure 2.4. The fundamental moment balance for the rock bags remains unchanged for these failure mechanisms, it is proposed to use the stability limit with a correction factor based on the test results.

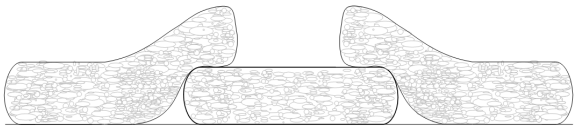

Figure 2.3: Diagram of rock bags in a grouped formation

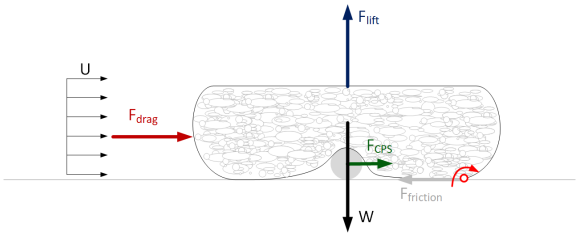

Figure 2.4: Free body diagram of a rock bag and CPS combination

2.2. Porous flow

For the interaction of a rock bag with water it is important to consider that it is not a solid structure, but rather a porous object. A hydrodynamic pressure gradient will cause a current in the voids between the rocks in the bag, u_{filter}. This will change the flow of water over the rock bag affecting the drag and lift force (Riezebos et al., 2021). The velocity is determined by the magnitude of the pressure gradient and the drag force. The pressure loss due to drag forces in porous media is described by the Forchheimer equation for the expected filter velocities in large granular material, such as the filling of rock bags (Ehlers, 2022):

$$I = au_{filter} + bu_{filter}^2 \tag{2.10}$$

With a the laminar flow drag coefficient and b the turbulent flow drag coefficient. Van Gent (1995) developed a model based on the Navier-Stokes equations and empirical experiments for these coefficients in oscillatory flow:

$$a = \alpha \frac{(1-n)^2}{n^3} \frac{\nu}{gd_{50}^2} \tag{2.11}$$

d_{50} of the granular material is the diameter exceeded by 50% of the material measured by mass. n is the porosity of the bulk material.

$$b = \beta(1 + \frac{7,5}{KC_p}) \frac{(1-n)}{n^3} \frac{1}{gd_{50}} \tag{2.12}$$

The porous Keulegan–Carpenter number KC_p is defined by the filter velocity, oscillation period T, porosity n and the diameter of the rock material d_{50}:

$$KC_p = \frac{u_{filter}T}{nd_{50}} \tag{2.13}$$

Van Gent (1995) found the material coefficients $\alpha = 1000$ and $\beta = 1.1$. In more recent numerical simulations these coefficients vary depending on research methodology and conditions (Jensen et al.,

2014, Losada et al., 2016). Lara et al. (2011) developed a calculation method based on flow over a porous bed, also based on the optimal results in a numerical simulation. For this study the empirical coefficient values by Van Gent (1995) are used to calculate the filter velocity in the rock bag u_{filter}.

2.2.1. Pressure gradient

The magnitude of the hydrodynamic pressure gradient is difficult to determine for a complex submerged structure like a rock bag. An upper and lower bound for the amplitude of the gradient can be determined. The lower bound is the amplitude of the pressure gradient in a wave field. For linear wave theory this is defined as (Holthuijsen, 2007:

$$I = \frac{kH}{2} \frac{\cosh kt_{rockbag}}{\cosh kd} \tag{2.14}$$

Where $t_{rockbag}$ is the height of the centre of the rock bag above the bed, k the wave number d the water level and H the wave height.
For the upper bound of the pressure, complete dissipation of the wave orbital velocity is assumed. This means that the velocity at the upstream end of the bag is equal to the amplitude of the orbital velocity, while at the downstream end, it is zero. With the dynamic pressure $q = \frac{1}{2}\rho u^2$ the pressure gradient is:

$$I = \frac{u_{orbital}^2}{2D_{bag}g} \tag{2.15}$$

In the scaling calculations for the rock bags the upper bound value is used.

2.3. Flow around a monopile and development

This section presents a discussion based on literature of the flow around a monopile and the effect on a rock bag placed to stabilise the CPS. The flow regime around a monopile consists of four components: streamline contraction, upstream down-flow, the horseshoe vortex and lee-wake vortexes (Schendel, 2018).
Streamline contraction causes acceleration of the flow near the monopile. In the horizontal plane, without considering vertical differences in velocity the flow amplification can be expressed analytically with a potential flow model (Miles et al., 2017):

$$u_r = u_\infty (1 - \frac{R^2}{r^2}) \cos\theta \tag{2.16}$$

For the radial flow component u_r. With $R = \frac{1}{2}D_{pile}$ the radius of the pile, r the distance from the pile's centre and θ the angle around the pile from the upstream direction. u_∞ is the original flow velocity far from the pile. The amplified velocity tangential to the pile:

$$u_{tangent} = -u_\infty (1 + \frac{R^2}{r^2}) \sin\theta \tag{2.17}$$

Finally, the total velocity:

$$u_{amp} = \sqrt{u_r^2 + u_{tangent}^2} \tag{2.18}$$

For the considered test set-up with half a monopile with a radius of 0.125 metre on one side of the flume of 0.76 metre wide. The maximum amplification is $\approx 3\%$ at the opposite wall of the flume.
Rock bags are placed at the touchdown point of the CPS on the scour protection. In this study this is assumed to be at approximately half a pile diameter from the edge of the monopile $R = D_{pile}$, the amplification there is ≈ 1.25. This does not include the effects of vortexes and turbulence that may further increase the amplification. Schiereck and Verhagen, 2019 give a figure based on the work by Melville and Raudkivi (1977), from this the approximate flow amplification factor near the rock bags is in the range 1.2-1.5. The height step of the scour protection can also influence the flow near the monopile and might further increase the turbulence (Petersen et al., 2015).

The horseshoe vortex forms close to the bed due to the down flow on the upstream side of the pile. It follows the pile downstream, mostly effecting the area close to the perimeter. The development of the the horseshoe vortex and lee-wake vortexes depends on the characteristics of the flow. These

can be described by the ratio of drag forces over inertial forces expressed with the KC number for the monopile:

$$KC_{pile} = \frac{uT}{D_{pile}} \tag{2.19}$$

With the amplitude of the velocity signal u, and the period T. Sumer and Fredsøe (1997) have determined that in wave only conditions, a horseshoe vortex will only form when the velocity causes larger values than $KC = 6$.

Shedding of the lee-wake vortex can be observed for flow Reynolds numbers where $Re > 40$ (Schendel, 2018) and in wave only conditions for $KC > 6$ (Sumer and Fredsøe, 1997). It is not certain how well the half pile will represent the lee-wake vortexes. Shedding is caused by the mixing of flows from both sides of a cylinder, so the wake of half a cylinder could be different. As a result, rock bags are not placed close to the side walls or the wake area in this study.
Further observations from literature include an increase in the turbidity in the wake region in a combined wave-current condition (Roy et al., 2018) and the monopile effecting the surface elevations in a wave field around the pile (Herdayanditya et al., 2024).

In conclusion, at the location of a rock bag placed for CPS stabilisation there is flow amplification due to acceleration of the flow around the monopile and turbulence. The amount of amplification depends on the exact location, flow characteristics and turbulence. The CPS is forced by a variety of sources of turbulent flow around the monopile (Miles et al., 2017). This means the load on the CPS and especially the load transferred by the CPS on a rock bag placed for stabilisation is difficult to determine.

3

Scaling

Two distinct scales are used to detect potential scaling effects. Primarily, to detect a loss of stability at one of the scales. That could indicate that the used stability calculation is not valid regardless of the dimensions. For practical purposes, 1:40 and 1:30 are used as scales in the experiments. The larger scale is limited by the ability to generate failure conditions using the available facilities. The lower scale is determined by the available fill material and mesh material for the bag. These scales also provide practical dimensions for other scaled models, such as the monopile and CPS.
For scaling in model experiments it must be demonstrated that the model provides a conservative estimate for the prototype stability. Thus, conservative scaling means that scaling effects at model scale are unlikely to overestimate stability at prototype scale.

Scaling is done by Froude's law; this method ensures that dynamic forces are consistent at prototype and model scales. Spatial dimensions are scaled linearly: a 3 metre diameter rock bag becomes $3/40 = 0.075$ metre. At model scale the viscous force of the water is not scaled down. So, the ratio of inertial and viscous forces decreases, which can be accepted as long as viscous forces remain negligible compared to the inertial force. The ratio is expressed by the Reynolds number, that predicts the turbulence of the flow. For the considered orbital velocities, rock bags and monopile dimensions, the Reynolds numbers are $> O(10^5)$. Although two orders of magnitude smaller than at prototype scale, this is deemed sufficiently turbulent (Riezebos et al., 2021). In figure 3.1 the main dimensions considered for scaling can be seen.

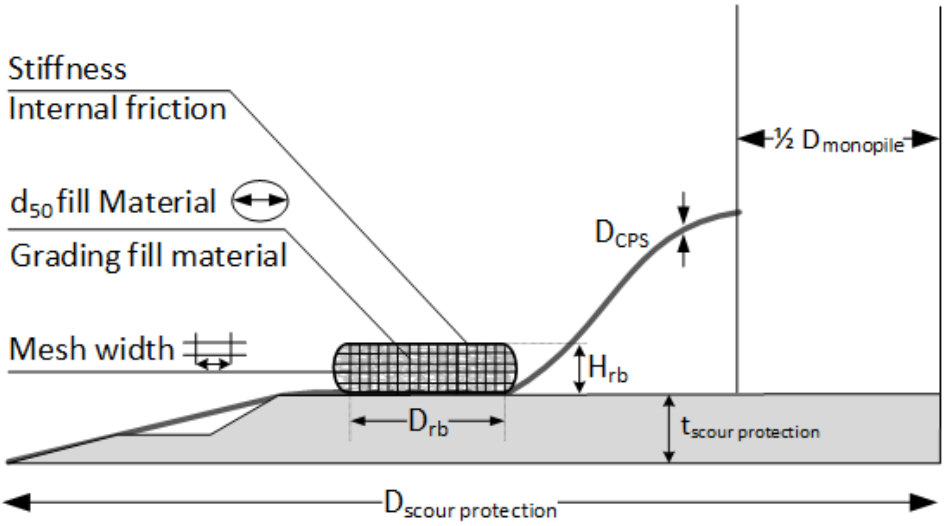

Figure 3.1: Schematized overview of the model of rock bag, monopile and CPS, with the main parameters for scaling.

3.1. Rock bags

The parameters that determine the dimensions of the rock bag are the diameter, height and shape. Manufacturers schematize the rock bags as an 'ice hockey puck', or 'sjoelschijf', cylinders with straight vertical sides. Alternatively, as with slightly elliptical sides (Ridgeway, 2024, Cirtex, 2023). In all pictures of prototype rock bags the edges seem to be more elliptical than straight. The prototype scale dimensions of the two types of considered rock bag can be seen in in table 3.1.

rock bags	Diameter [m]	Height [m]	Volume [m^3]
4 ton	2,4	0,6	2,7
8 ton	3	0,7	5

Table 3.1: Manufactures specified dimensions of the considered rock bags

Examining the dimensions of the model bags, such as their weight, shape, and height-to-diameter ratio, is an important way to determine whether or not similarity in scaling has been achieved. In this case, the model bags should have similar properties to those at prototype scale. For a description of the fabrication process see appendix A. In general, the smaller rock bags are harder to have matching shapes, so for the desired diameter the height matches better for the larger bags. The diameter is made such that the outer line of the bags just overlaps the target diameter when looking from above, but when the point of view is slightly changed the line is visible.

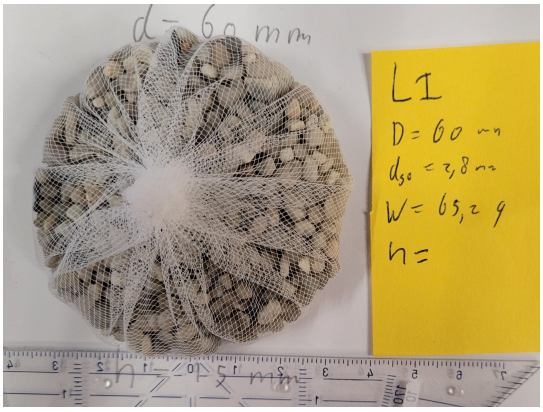

Figure 3.2: Top view of bag L1

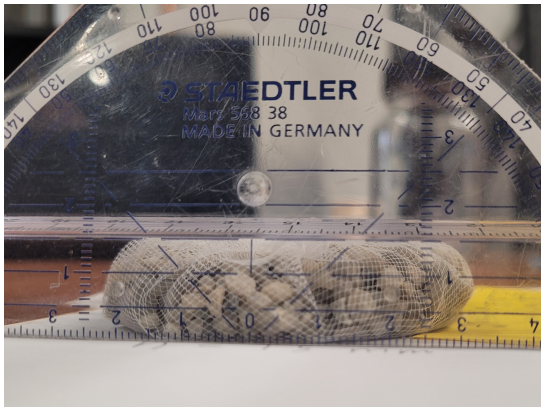

Figure 3.3: Side view of bag L1

Rock bag	Type	Weight [g]	Diameter [mm]	Height [mm]	Target height [mm]	d_{50}/D [-]	d_{50}/H [-]
S1	1 to 40; 4 ton	62.5	60	15	15	3.2	0.13
L1	1 to 40; 4 ton	62.5	60	15	15	4.7	0.19
S2	1 to 30; 4 ton	148	80	20	20	2.9	0.12
L2	1 to 30; 4 ton	148	80	20	20	4.1	0.17
N1	1 to 40; 4 ton	62.5	60	15	15	3.2	0.13
N2	1 to 30; 4 ton	148	80	20	20	2.9	0.12
S3	1 to 40; 8 ton	125	75	20	17.5	3.1	0.12
L3	1 to 40; 8 ton	125	75	20	17.5	4.4	0.17
S4	1 to 30; 8 ton	296	100	25	23	4.1	0.12

Table 3.2: Overview of normal density rock bag dimensions

3.1.1. Mesh material

At prototype scale, bags are made from polyester lines with a mesh of 25 mm for the four ton bag and 50 mm for the eight ton bag. Some of the specification sheets show two parallel lines (Ridgeway, 2024). The diameter of the lines and the elasticity of the material are unknown. Cirtex (2023) specify a maximum tensile strength of the net and a deformation at maximum load for 'a single net'. It is not clear if the deformation of the mesh is taken into account or how many lines make up a single net.

If it were possible to perfectly scale the mesh material, this still would not mean that such a material is available. So, an as-flexible as possible material is chosen, with a mesh size that is just small enough to hold the smallest fill material fraction without leakage. The material chosen is Thule also known as wedding veil. A flexible mesh material made from nylon, similar to what Coghlan et al. (2024) used. On average, nylon has smaller elasticity compared to polyester. But, for all polymer materials, this value can fall in a wide range. Some experiments were conducted with a bag made of slightly different material with a larger mesh; this did not result in any different behaviour.

3.1.2. Fill material

To assess the influence of fill material size on the stability of rock bags, the fill material size is varied. Two sizes of fill material are used for both bag types: the manufacturer's specified d_{50} and a larger size. For the four-ton bag, the larger size is double the specified d_{50}. For the eight-ton bag it is 5/3 of the specified d_{50}. This smaller increase ensures the diameter-to-height ratio of the bag does not exceed 1 to 5, maintaining the integrity of the rock bag. The tested range of fill material diameter relative to bag diameter at prototype scale is $2.1\% < d_{50}/D_{bag} < 4.2\%$. The ratio of d_{50} to bag height ranges from $8.3\% < d_{50}/H_{bag} < 17.9\%$. Table 3.2 presents the scaled rock bag ratios.

For a valid comparison, the behaviour at model scale has to be similar to prototype scale. The fill material is scaled as proposed by Riezebos et al. (2021). The theoretical mobility of the fill material at model and prototype scale is kept equal using to the mobility definition by Dixen et al. (2008) and the critical Shields parameter θ_{cr} by Soulsby (1997). This results in particle diameters that are up to 30 to 50% larger compared to length scaling, due to the slightly lower density of gravel in the lab ($\rho = 2500kg/m^3$), the lower density of fresh water compared to salt water and a lower critical Shields parameter for the model fill material. Figure 3.4 shows the positions of the model and prototype scale material on the Shields curve. Dixen et al. (2008) proposes a maximum $\theta_{cr} = 0,045$ for material with $d > 10mm$ compared to $\theta_{cr} = 0,055$ in the original formulation. This reduces the difference between the length-scaled and mobility-scaled sizes for larger material.

For practical purposes the d_{50}'s of the bags differ slightly to reduce the number of different fill materials needed and account for the available sieve sizes. See table 3.3 for a comparison of the length-scaled and mobility-scaled fill material. The gradings of the designed fill material can be found in appendix A.2.

Critical hydraulic conditions for the rock bags are used in all scaling computations: a near-bed velocity amplitude of 3.4 m/s and a period of 13 seconds at prototype scale. The velocity is based on the steady current limit for a four-ton bag (Ridgeway, 2024), and the period is selected for a wave that could generate such a velocity amplitude.

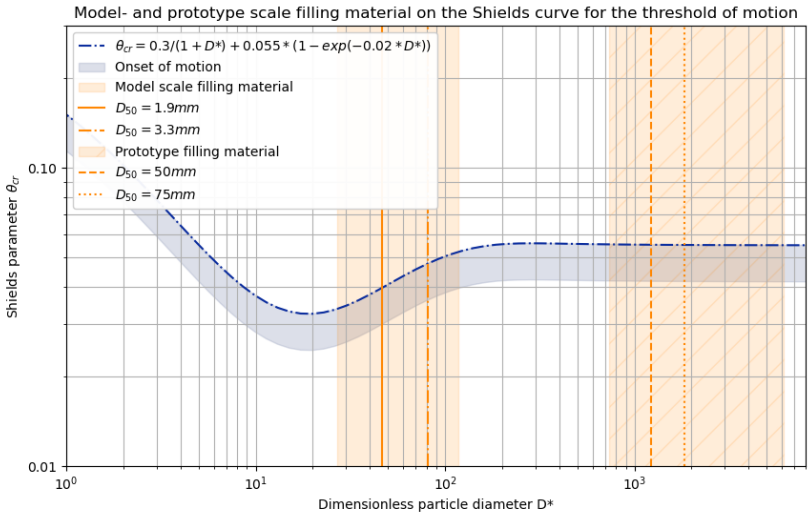

Figure 3.4: Model and prototype scale fill material placed on the diagram for the critical Shields parameter for mobility

Bag number	Scale	D_{50} [mm]	D_{50} Froude scale [mm]	Porosity	u_{filter} ratio model / prototype [-]	Laminar / turbulent resistance au/bu^2 [-]
S1	1 to 40	1.9	1.25	0.46	0.18	45
L1	1 to 40	2.8	2.5	0.46	0.36	17
S2	1 to 30	2.36	1.67	0.46	0.23	30
L2	1 to 30	3.35	3.3	0.46	0.30	12
N1	1 to 40	1.9	1.25	0.40	0.09	76
N2	1 to 30	2.36	1.67	0.40	0.12	50
S3	1 to 40	2.36	1.88	0.46	0.24	28
L3	1 to 40	3.35	3.1	0.46	0.44	11
S4	1 to 30	2.8	2.5	0.46	0.29	20

Table 3.3: Overview of the normal density rock bags used in the experiments. S indicates small fill material, L large fill material, and the bags indicated with N have a porosity comparable to the prototype bag. The second to last column shows the percentage of the maximum filter velocity at model scale of the Froude scaled prototype filter velocity.

3.1.3. Porosity

The goal of this part of the research is to find a correct representation at scale of the part of the forces exerted on the bag by the current and waves, within the bag. The current and pressure gradient drive a flow through the porous rock bag. When this filter velocity at model scale is equal to the Froude scaled velocity at prototype scale, this would result in equal dynamic forces.

At model scale there is a large influence of the size of the fill material on the magnitude of the filter velocities. If the size of the fill material is chosen in order to achieve filter velocities that are equal to the Froude scaled filter velocities at prototype scale, this results in unacceptably large fill material.

There are two possible explanations for the effect of too low filter velocities. It may result in conservative force on the model bag due to increased dynamic pressure against the bag's frontal area, as there is less transmission into the bag. According to Coghlan et al. (2024), lower filter velocities at model scale reduce the force exerted by this current on internal material. In this case, model bags with low permeability would not be not conservative.

The porosity of the fill material can be adjusted by grading the particle sizes. A narrowly graded material will have higher porosity. This is intuitive because when size differences are small, smaller particles do not fill the gaps between larger particles. This adaptation is made to ensure that the ratio of model filter velocities to Froude scaled prototype filter velocities is not too small. A very narrowly graded material has a porosity of 0.46. Because, the laminar resistance is much higher at the model scale, complete similarity with the prototype scale is impossible. Calculation for the theoretical porosity is based on the Rock Manual (CIRIA, 2007), with $e_0 = 0,94$. Using a ratio for $d_{85}/d_{15} = 1,2$ the porosity of material is 0,46. This is close to the maximum porosity for heterogeneous material. The filter velocities are calculated with the method outlined in section 2.2.

In theory, the bulk density is lower for higher porosity material.To achieve the same rock bag weight, more volume is needed. Since the rock bag diameter is important for the stability this is not changed nor is the height of the rock bag. The additional volume will be achieved through a change in the shape of the bag. Volume can be gained by shaping the bag more like an ellipsoid, though the impact is unclear as the drag coefficient can be influenced by shape. The lower bulk density of the bag might also impact the stability. In the original derivation of the limit by Jacobsen et al. (2023) the porosity is a factor, but this was disregarded by them due to the low variance of the porosity in their study.

To investigate the effect of the adapted porosity, two 4 ton bags with mobility scaled fill material are tested with grading and porosity values similar to prototype bags, N1 and N2. These have the same mobility, according to the limit by Jacobsen et al. (2023). Table 3.3 summarises the chosen bags and the ratios of filter velocities and laminar to viscous resistance.

3.1.4. Internal friction

The ratio of volume and thus weight compared to the surface area is determined by the diameter:

$$\frac{V}{A} \sim \frac{D^3}{D^2} \sim D \tag{3.1}$$

And the inter particle friction force is dependent on the area of contact:

$$F_{friction} \sim D^2 \tag{3.2}$$

This means that as fill material of rock bags is scaled down, the relative friction force to particle weight increases. As a result, inner particle drag is reduced. Furthermore, the material strength of protruding parts of rock will be insufficient to withstand movement at prototype scale, and such features will break. At model scale, using as round materials as feasible could mitigate part of this effect, as more circular particles have less surface area and protruding elements. Internal friction is especially important for rock bags because it impacts reshaping of the bag caused by fill material movement during loading. This determines how rigid the rock bag responds to overturning forces.
In order to test the hypothesis that the internal friction of the filling material has an important role in the stability and failure mechanism of rock bags a limit case was sought. Four bags were made filled with perfectly round glass spheres. These have very limited internal friction. Glass has a similar density to the rocks used in these experiments $\rho = 2500kg/m^3$. The theoretical porosity of randomly placed equal rigid spheres n=0.365 (Wu et al., 2003), lower compared to wide graded rock fill material. Binary particle material have a lower porosity, that can go to n=0.32 for larger ratios between particle sizes (Brouwers, 2023). An overview of the glass filled bags is shown in table 3.4. Figure 3.5 compares the shape of prototype and model bags while suspended. Internal friction is clearly affecting the suspended shape of the bags.

Bags	d_{50} [mm]	Weight [g]	Diameter [mm]	Height	d_{50}/D [%]	n [-]
G1	1.9	62.6	60	15	3.2	0.365
G2	4	62.4	60	15	6.7	0.365
G3	50% 1.9 / 50% 4	62.6	60	15	4.7	0.32
G4	55% 1.9 / 45% 4	125	75	18	3.8	0.32

Table 3.4: Overview of glass spheres filled bags used for testing.

Figure 3.5: Suspended prototype scale rock bag

Figure 3.6: Suspended 1 to 40 narrow graded rock bag S1

Figure 3.7: Suspended 1 to 40 1,9 mm glass spheres filled bag G1

Figure 3.8: Suspended 1 to 40 4 mm glass spheres filled bag G2

3.2. Full model

The scaling of other components in the model has been done considering the length scale and practical limitations.

3.2.1. Monopile

Constricted by available sizes in piping, chosen for the more easy to get PVC pipe instead of transparent acrylic pipes seen often in hydraulic engineering labs. This was possible because of the camera positions. The opaque pile also makes the position of the bags relative to the pile more visible and increases contrast in the video recordings. A 250 mm diameter pipe is chosen. At 1 to 40 scale, a 10 m prototype foundation is modelled and for 1:30 scale the prototype diameter is 7,5 m. This diameter also is small enough so flow amplification is low, max 3 % at the opposite flume wall and similarly limited influence of the wall on the flow pattern around the pile

3.2.2. Cable protection system

The model of the cable protection system is designed based on limited information about dimensions on prototype scale. These systems are highly variable per wind park and structure, as they are not standard products but designed specifically for each project. In the context of this research, the most important parameters of the CPS are the diameter, weight and stiffness. The diameter depends on diameter of the power cable that is protected. The stiffness of the CPS depends on the location and is also different for each project. For example, the cps is made less stiff further away from the monopile in order not to cause unnecessary loads on the cable. At model scale the stiffness of materials is usually too large, because the moment of inertia scales with $O(10^5)$. So an as flexible as possible cable is used.
The CPS is modelled by a rubber-coated electrical wire. The properties of the model CPS and the translation to prototype depending on the scale are shown in table 3.5. The stiffness of the cable was not measured, but it had no problem getting into the desired shape.

Scale	Diameter [mm]	Weight [kg/m]	Density [kg/m3]
model	8.6	0.1125	1936
1 to 30 prototype	258	101	1936
1 to 40 prototype	344	108	1936

Table 3.5: Comparison of model and represented prototype prototype CPS

3.3. Hydraulic conditions

For the design of the hydraulic conditions, 50-year design conditions at four wind parks built by Van Oord in the North Sea and Northern Atlantic have been consulted. They are in water depths between 23 and 38 metres. In the lab, a distorted depth will be used in order to generate as large as possible orbital velocities to be able to achieve mobility of the rock bags. As a result, the waves are longer compared to the water depth then at prototype scale. This could mean the waves are more non-linear, increasing the influence of second order effects. In many physical model studies only the linear orbital velocity is taken into account. If the Ursell number in the lab is greater than at prototype scale, this might be conservative, because the actual peak orbital velocity in the lab will be larger due to the higher order effects, although the period of this peak flow is shorter.
Especially for the North Sea wind parks, wind waves are thought to be dominant, with periods that are relatively short compared to the wave height. An overview of the design wave conditions can be seen in table 3.6. Locally, depth induced wave breaking can occur in some of the wind parks.
All irregular wave spectra are with $1.4 < T_p < 3.7$ and $H_s < 0,21m$. This is within the limits of the wave maker, but not all expected wave heights are exactly reached, due to depth and steepness induced breaking. The average JONSWAP setting of the wave maker is used for the shape of the spectra. The peak periods used are the scaled periods of the wind park conditions: 1.8, 1.9, 2.2, 2.1, 2.5, 2.9, 3.4. Some periods in between are also used and for the tests during the conference a few additional periods outside the range of these scaled wind park periods were used.

Wind parks	Water depth [m]	Peak period [s]	H_{m0} [m]	Ur H_{m0} [-]	$H_{2\%}$ [m]	Ur $H_{2\%}$ [-]	U2 linear orbital velocity [m/s]	Maximum steady current near bed velocity [m/s]
1	22	12.2	7.5	18.3	11.0	26.8	2.94	0.8
2	23	11.5	7.3	14.0	10.7	20.4	2.67	0.9
3	38	18.5	8.8	17.5	12.9	25.6	2.78	1.5
4	28	15.6	9.4	24.4	13.7	35.6	3.42	1

Table 3.6: Wave conditions and corresponding Ursell numbers at prototype scale

The scaled 1 to 40 $H_{2\%}$ linear orbital velocities of the wind park conditions are in the range $0.42 < u_{lin} < 0.54$ m/s, for scale 1 to 30 the $H_{2\%}$ orbital velocities are the range $0.48 < u_{lin} < 0.62$ m/s. In the model tests with a monopile on 1 to 40 scale the $H_{2\%}$ orbital velocities are in the range $0.19 < u_{lin} < 0.56$ m/s. For tests on 1 to 30 scale the range of $H_{2\%}$ orbital velocities was $0.39 < u_{lin} < 0.63$. For most tests with waves combined with steady current a current of ≈ 0.14 m/s was used. Representative for three of the four wind parks. Slightly higher steady currents were possible, but caused distortion of the waves. In appendix A.3 the used irregular conditions are shown. The range of Keulegan–Carpenter

number for the linear orbital velocity of the 2% wave and the monopile $1 < KC < 8.4$. This KC number per condition can be found in the appendix.
An overview of the range of regular waves used in the tests is shown in table 3.7. Regular wave tests last about 85 seconds and for 20 to 55 waves depending on period and exact duration. As the bags could gain stability due them settling in the bed or getting more compact, they are lifted and slightly moved between each test, also the positions of the two or three bags are varied between the tests. Test conditions are stopped for regular and irregular waves at catastrophic failure. When all bags in the flume roll out of frame of the cameras.
For the combined wave-current tests in this study only wave dominated conditions were used. The limit for this is chosen to be $u_{current}/u_{w,lin} < 0,6$. This means the steady current velocities are small compared to the velocity needed for failure due to only steady current. The used current velocities are comparable to Froude scaled conditions at real wind parks, shown in table 3.6.

	Model		1 to 40		1 to 30		Ursell number
	T [s]	H [m]	T [s]	H [m]	T [s]	H [m]	[-]
Minimum Ursell number	1.49	0.189	9.42	7.56	8.16	5.67	7.68
Maximum wave height	2.59	0.328	16.4	13.1	14.2	9.84	53.1
Maximum Ursell number	2.99	0.295	18.9	11.8	16.4	8.85	65.5

Table 3.7: Overview of the range of used regular wave conditions at model and prototype scale with associated Ursell numbers.

4

Test set-up

The experiments are conducted in the hydraulic engineering laboratory of the faculty of civil engineering and geosciences of the Delft University of Technology. Figure 4.1 shows the set-up in the wave flume. The flume measures 36 metres in total length, 0.9 metres in height, and 0.76 metres in width. The flume has glass walls on both sides that are approximately 75 centimetres high. Wooden planks are placed on top of the flume to increase its height.
Waves are generated by a brand-new piston wave paddle, with active reflection compensation. A parabolic dampener is paced at the end of the flume, that allows for transmission of current. The flume is connected to a pipe circuit and a pump that can generate current in the direction of the waves. The inflow of the current is in front of the wave maker through a vertical opening that is about 10 centimetres high and 60 centimetres wide. The opening is created by raising the cover plate on one side.

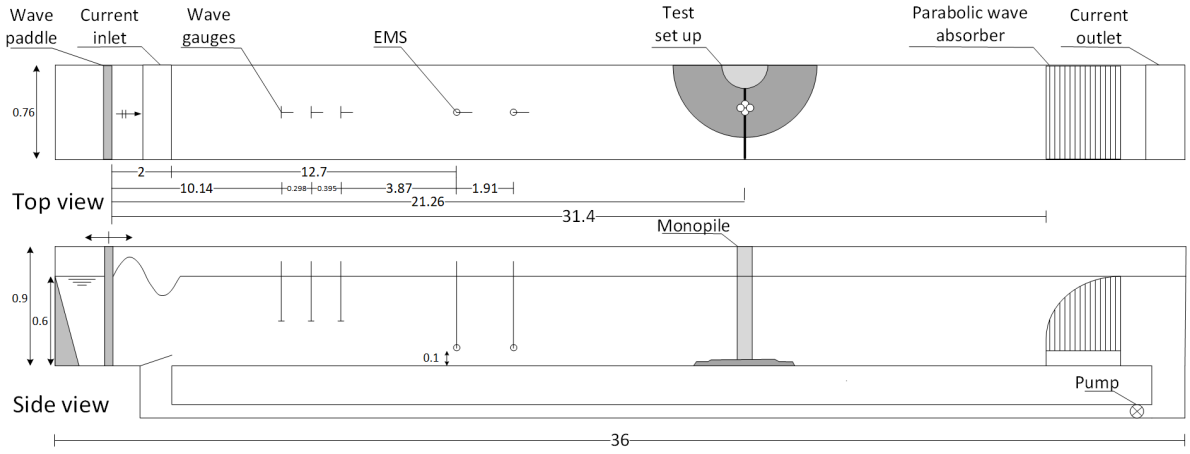

Figure 4.1: Top and side view of the experimental set-up in the flume distances in metres

For the experiments two model set-ups are used. The first is a flat rough bed that is 1.2 metres long, the width of the flume, and 30 millimetres high. The rough bed is made with a steel plate and rocks with a d_{50} of 8 mm glued to it with epoxy resin. A glued rough bed is chosen to ensure that there is no movement of the bed to influence the test results and to allow for additional tests, as there is no delay for bed repairs. The roughness is caused by the shape of the rocks, so the epoxy smoothing the rock's surface is not an issue, almost no sliding failure of the bags was observed.
The tests are carried out with two or three rock bags placed side by side, with their centres 25.3 or 19 centimetres apart. The rough bed is the same length as the diameter of the scour protection in the other model. The contrast between the black stones, white bag mesh, and grey stones of the fill material was adequate for the used image processing method.
The full model set-up consists of a scour protection, CPS and half-monopile. In the field, the cable is buried beyond the scour protection, the model CPS is taped to the bed to mimic this. The CPS is

pulled through the pile and attached to the top of the flume. A screw through the cable at the entry point prevents the cable from penetrating further into the pile and losing its desired shape. The monopile is placed in the scour protection, where a space with the same diameter as the pile is left. The pile is attached to the flume wall and held down by a cover plate on top. An additional clamping band is used to secure the pile to the bottom of the flume wall's wooden planks.
The dimensions of the scour protection are based on practical examples and are in line with Vos et al. (2011). The scour protection consists of a semicircle with a diameter of 5 times the monopile and approximately 10 millimetres thick, the filter layer. On top the armour layer is placed with a diameter of 3 times the monopile and approximately 20 millimetres thick. For simplicity both layers are made with the same rock material and the stones are glued together for the same reasons explained above. In figure 4.2 the cross section of the model is shown.

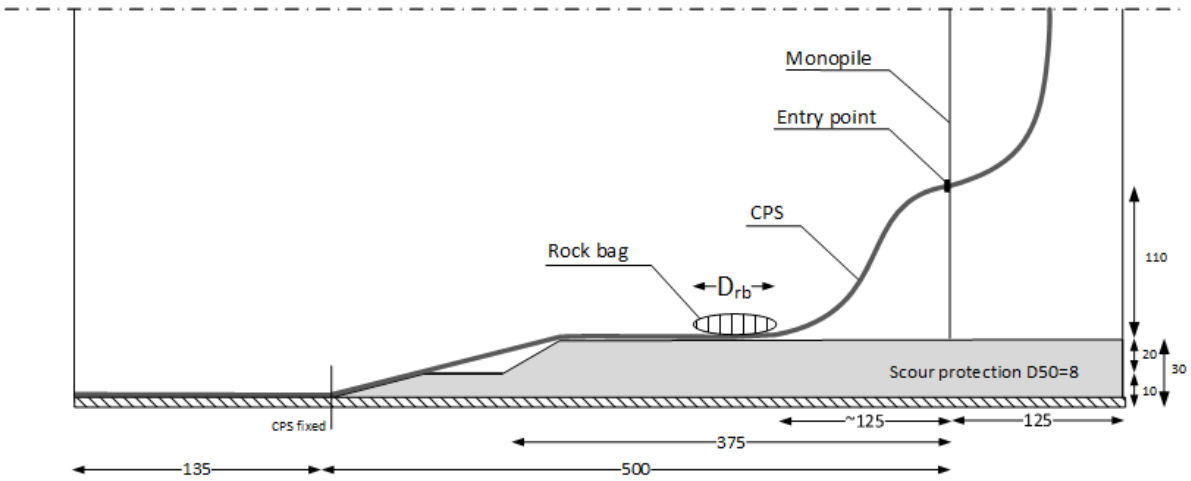

Figure 4.2: Detailed cross section of the full model set-up [mm]

On both the rough bed and scour protection the centre of the rock bags are at approximately 40 millimetres above the level of the floor of the flume. This height is used in all computations of orbital velocities for the rock bags. Although, there is limited difference with the theoretical wave orbital velocity at the bottom.
Wave height data is recorded with an array of three resistance type gauges 10 metres from the wave maker. Velocity data is recorded by two electromagnetic fluid velocity meters (EMS). These are placed at more than 10 metres from the outlet in order record the developed flow and there is a two metre gap between the devices in order to be able to spot differences in flow that could indicate the flow not being fully developed. The gap also reduces the effect of turbulence by the other measurement devices.

5 Results

The results of the tests are discussed in this chapter. An overview of all conducted tests and a description of the methodology can be found in appendix C. The observed failure mechanism of rock bags is presented in the first section. In the second section, the analysis of before and after top pictures is explained. The observed movement in the top pictures is related to the analysis of the failure mechanism to determine a failure criterion.
The sections that follow discuss the observations and results from the various types of tests, as well as the influence of the most important parameters. The wave data analysis is summarised; however, appendix D contains more detailed information about the used methodology.

5.1. Failure mechanism

Based on the observed response to loading of rock bags in the tests four levels of movement of rock bags are described. After a number of waves, one level of movement can escalate into the next. Movement of internal material occurs on all levels of movement. An illustration of these levels of movement is provided in Figure 5.1.

1. Movement of internal material, only local reshape of part of the bag;
2. Uplift of part of the bag, bag might be shifted or reshaped;
3. Rocking of the entire bag around its centre, this can lead to 'walking away' of the bag;
4. Overturning of the bag around a point in contact with the bed, this will lead to either overturning or walking of the bag.

Level 1 and 2 can be classified as stable when only locally occurring, when it results in reshaping of the entire bag it is classified as rocking, level 3 can either be rocking or failure depending on the amount of movement. If level 4 movement is observed it is always classified as failure.
Bags take a number of waves before reaching failure, in general failure occurs after a lower number of waves for higher ψ value conditions. In most tests there is some motion of internal material at the front of the bag, in many tests the motion subsides or stops as the test progresses. Some short-period waves cause the bags to shake slightly, but not enough displacement to be visible in the top picture comparison.

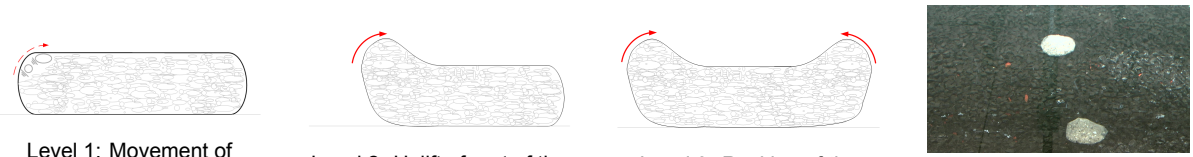

Level 1: Movement of internal material

Level 2: Uplift of part of the bag

Level 3: Rocking of the entire bag

Level 4: Overturning bag as seen during the tests

Figure 5.1: Schematized levels of movement 1 to 3 and an example of an overturned bag during the tests

5.2. Classification of stability

The classification of the tests is based on the observed change in position of the rock bag in the before and after picture. A heat map of the differences between those to pictures is made for each test, see Figure 5.5. Three classes are used: stable, rocking and failure. A bag is classified as rocking when there is a change of position on at least two sides of the rock bag. Otherwise, there was only movement of some fill material during the test that changed the edge position of the bag at one side; this is classified as stable. When the displacement of the bag exceeds one-sixth of the diameter of the rock bag, it is classified as failure. This is approximately equal to the diameter of a CPS. The side video is also visually analysed to classify a rock bag's performance in tests. If only level 1 or 2 movement can be seen in the video, the rock bag is classified as rocking. If the top picture analysis shows limited displacement but video level 3 or 4 shows movement, the classification is failure.
In appendix B, more examples of the top picture-based classification can be found for most types of tests.

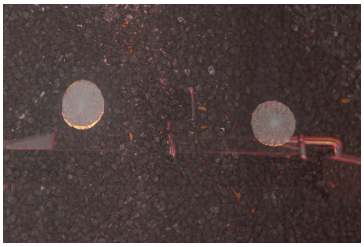

Figure 5.2: Regular wave test R45, left: Rocking, right: Stable

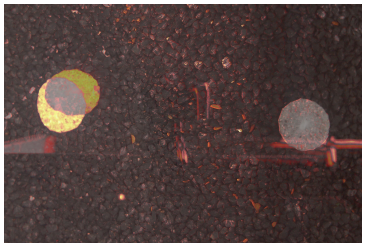

Figure 5.3: Regular wave test R50, left: Failed, right: Stable

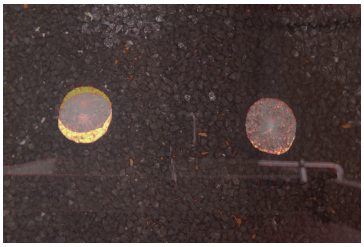

Figure 5.4: Regular wave test R108, left: Failed, right: Rocking

Figure 5.5: Heat map of difference of before and after picture over the before picture in three tests

5.2.1. Grouped bags

For grouped bags, the classification is mostly similar. In some cases, only one exposed bag shows movement while the rest of the formation is stable. When one bag, not in contact with the CPS, exhibits some deformation but the formation remains intact and the cable has not moved more than one diameter, it can be classified as rocking. Because there seem to be no forces on the cable and the formation is intact, this is not failure. Failure occurs when at least one of the bags loses overlap with the formation, if the whole formation is shifted one-sixth of the rock bag diameter, or if one of the bags that would be in contact with the CPS is shifted one-sixth of the rock bag diameter.

5.3. Regular wave tests

In this section the the results of the regular wave tests are presented and the influence of varied parameters is discussed.
Due to the large influence of reflections for the high regular waves an analysis method is developed to account for the influence of these reflections on near-bed orbital velocity. The orbital velocity for the incoming wave is determined by fitting the 5th-order Stokes wave to the leading waves of the measurement. In these leading waves no reflected signal has arrived at the wave gauges. The reflection was determined by subtracting this signal from the total wave signal. Next, the spatial and temporal interference pattern of the final standing wave can be reconstructed. This method was checked with velocity measurements that were performed at two locations between the set-up and wave gauges. For the tests with a reasonable increase in constructive interference at the set-up, the increased velocities of the combined signal were taken into account in the analysis. For the others the velocity amplitude of the fitted wave to the leading waves is used. A more detailed explanation of the analysis method can be found in appendix D.

In Figure 5.6 all results for normal density rock filled bags are shown in a scatter plot manner. Jacobsen et al. (2023) hypothesised an end to the dependence of stability on KC beyond $KC = 15$. When the limit is extended for $15 < KC < 25$ with $\psi_{cr} = 0.225$ as suggested in the recommendations of Jacobsen et al. (2023) a reasonable lower bound for the onset of failure can be seen in the data. Indicated in

Figure 5.6 are the tests mentioned in the analysis appendix D as well as a number of outliers, that are discussed in this section.
Negative outliers, failed bags below the limit:

- R12: Only one of the bags (S1 fails), the other (L1) is rocking. There are constant measured current amplitudes that are slightly higher than the fitted wave and combined currents at the EMS locations. The combined velocity amplitude is just larger than the fitted wave amplitude. It is deemed a trustworthy result, although the measured velocities exceeding the calculated ones at the EMS locations indicates that the velocity amplitudes experienced by the rock bags might have been larger than the calculated ones.
- R26: Only L1 fails, S1 is rocking. There is a very large difference between the magnitude of velocity amplitudes for the two EMS', so is a strong spacial dependent interference. The calculated combined velocity amplitude is not accurate at the location of the first EMS. At the set-up location the combined incoming and reflected amplitude is lower than that of the fitted wave. The fitted wave velocity amplitude is therefore used.
- R108: In this test bag S3 failed and L3 was rocking. At the set-up location the combined amplitude is lower than that of the fitted wave. The fitted wave velocity amplitude is therefor also used in this test.

Positive outliers, stable bags for $\psi > 0.3$:

- R46: Both S1 and L1 are stable in this test. The combined incoming and reflected amplitude at the set-up is 111% of the fitted wave velocity amplitude. At the EMS locations both are larger than the measured velocity amplitudes, but smaller than at the set-up.
- R316: This test is an outlier for the N1 bag that is classified as stable. For the also stable and larger N2 bag the KC and ψ values are smaller. The combined velocity amplitude at the set-up is 110% of the fitted wave and both are larger than the measured velocity amplitude at the EMS' locations, but the difference is smaller than in the previously mentioned test.

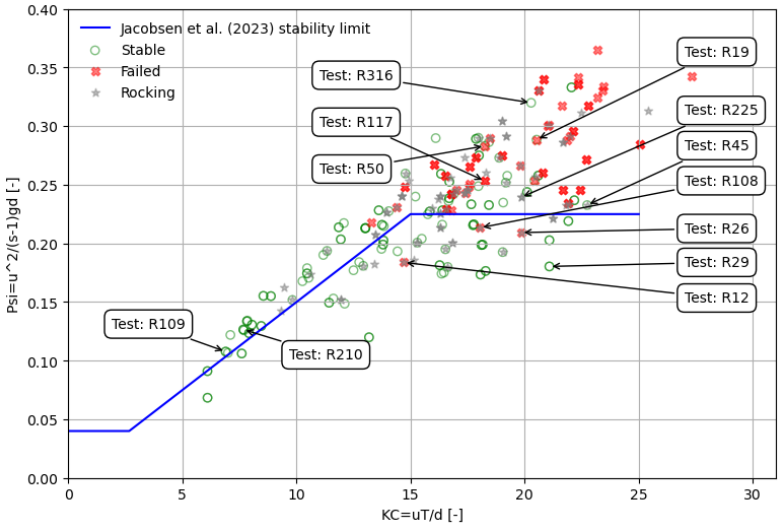

Figure 5.6: Scatter plot of the results of regular wave tests, with indicated test numbers. Compared to the extended Jacobsen et al. (2023) stability limit. For $s = \frac{\rho_{rock}}{\rho_w}$ and u based on the amplitude of fitted or combined orbital velocities

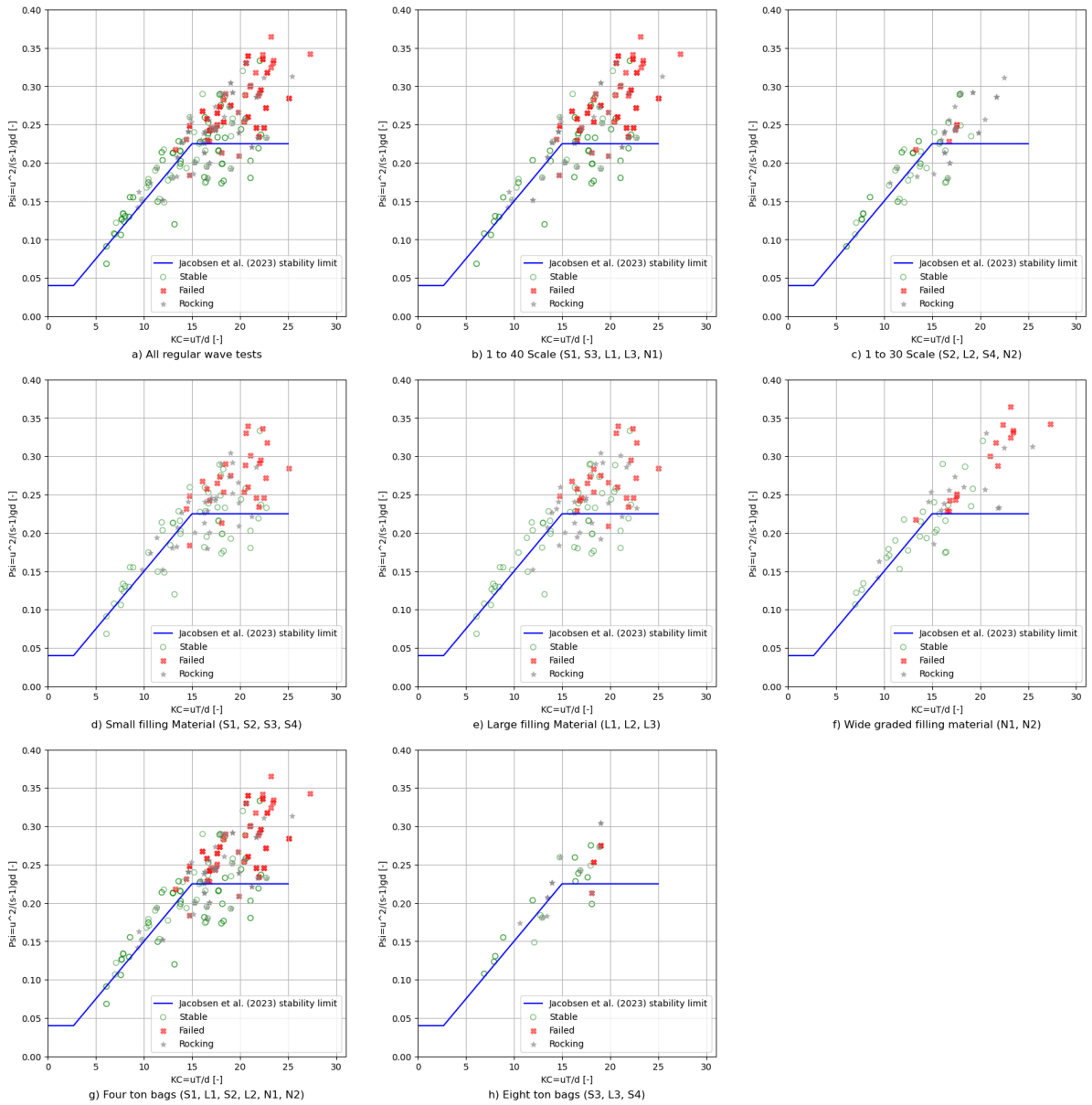

Figure 5.7: Results of all normal density material regular wave tests split for relevant parameters. Compared to the extended Jacobsen et al. (2023) stability limit.

5.3.1. Scale and rock bag size

With the facilities at hand it proved more difficult to reach failure for the 1 to 30 scale. The results for these bags can be seen in Figure 5.7 c. In the rough bed regular wave tests failure was only observed for the 1 to 30 four ton bags S2 and L2. Since there are failures for these bags around the stability limit, it is found to be similarly representative as for the 1 to 40 scale. There is definitely no indication that there is a loss of stability at this larger scale. A similar observation can be made for separated the eight ton bags, see Figure 5.7 h.

5.3.2. Filling material size and grading

The results for different filling materials are split up in figures 5.7 d, e and f. At a glance, there are no large differences. The results from tests with direct comparison of the bag types are shown in table 5.1. As a result, the same picture emerges. Although the large filling material bags might show a bit more stable behaviour, the stability limit seems to be a satisfactory estimate for all three filling material types in regular waves. Only a few tests directly compare the narrow and wide graded filling materials, yet

Bag type 1	Bag type 2	Failure bag type 1	Failure bag type 2	Failure both types	total tests
Small material	Large material	8	5	21	105
Narrow grading	Wide grading	2	1	3	6

Table 5.1: Tests with direct comparison for different filling material sizes and gradings.

the scatter plots reveal a similar onset of failure.

5.3.3. Low density filling material

The waves used in these experiments were more linear. The used fitting method in the analysis sometimes over predicts the peaks and troughs of the waves. Although, the estimates for the fitted wave orbital velocity amplitudes seem to correspond well at the EMS locations, being slightly larger. In 13/29 tests the combined orbital velocity was more than 115% of the fitted wave and thus the fitted wave velocity was used.
In general high mobility of the fill material was observed. As there was movement of fill material around the edges even when there was no movement of the whole bag visible in the videos. Because of this, bags sometimes have to be classified as rocking, when the centre of the bag moved very little.
The very small filling material makes the bags very stiff, this could cause a scaling effect as the observed failure mechanism is more rigid. This is also seen in the slope tests in Section 5.7. In these tests the low density bags were most stable. The rigid movement is mainly seen for the larger bags, where the ratio of fill material diameter and bag diameter $\frac{d_{50}}{D_{bag}}$ is smaller. According to these tests, the stability limit appears conservative in this region, but over prediction of the crest level and too rigid failure may play a role. An overview of the used bags can be seen in table A.1 in appendix A.

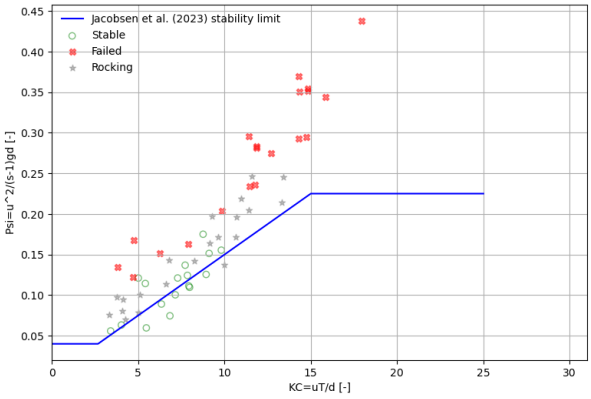

Figure 5.8: Scatter plot of the results of regular wave tests with low density fill material $\rho = 1500kg/m^3$. Compared to the extended Jacobsen et al. (2023) stability limit.

5.3.4. Glass material tests

The tests are analysed with the same method as other regular wave tests. The wave fields used in this research are on the lower energy side of regular waves. For most tests the fitted wave performs well. The observed failure mechanism is the same as for the rock-filled bags. This material also exhibits a rocking-type motion and a slight movement of the fill material at the front of the bag. There is a stronger shaking or jiggling motion of stable or rocking bags compared to the rock-filled bags. This motion can be felt when the bags are shaken by hand, unlike the rock-filled bags.
In Figure 5.9 the results of the tests are plotted. In general these bags are less stable compared to the rock-filled bags. In table 5.2 a direct comparison of stability can be seen. The bag with only small fill material G1 has the least stability. It fails multiple times below the stability limit. Failure for this bags starts from $\psi = 0.17$. The other bags are more stable as can be seen in the b plot and direct comparison table, but also have a decreased stability compared to the rock-filled bags. With nags G2 and G3 failing below the stability limit from $\psi = 0.185$. The larger bag G4 actually performs relatively well compared to the rock-filled bags, although only a few tests have been done, so no definitive conclusion can be drawn from this.

Bag type 1	Bag type 2	Failure type1	Failure type 2	Failure both types	total tests
G1	G2	3	2	11	26
G1	G3	4	1	10	26
G2	G3	4	2	9	26
G4	S3	1	0	1	5

Table 5.2: Direct comparison of tests with glass filled bags and similar size normal rock filled bag. Bag G3 with a wider grading scores marginally better than the others and G1 filled with only the smallest glass spheres worst. In the direct comparison the normal rock filled bag also performs better.

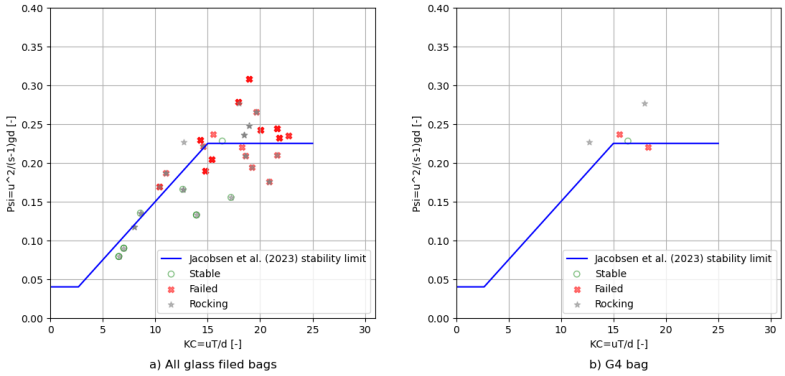

Figure 5.9: Scatter plot of the results of glass spheres filled bags. Compared to the extended Jacobsen et al. (2023) stability limit. For $KC > 14$ a lower stability of the smallest size bags is observed (G1, G2, G3), failure starting from $\psi = 0.17$ in that region.

5.4. Grouped formation tests

Four different formation types applicable for CPS stabilisation are evaluated. These are formations that can be made by placing one rock bag at a time. Theoretically formations are possible where bags are weaved together by placing multiple at a time. Due to the perceived difficulty of installing this offshore, these are not included in the study. The bags used for these experiments are the smallest low density fill material bag (FL1) and the 1 to 40 four ton bag (S1). The tested formations are shown in Figure 5.10. For all formations the same wave conditions are repeated, with assumed similar resulting forces on the bags. The formations are evaluated based on the performance in these conditions, this evaluation is shown in table 5.3 for the low density bags and table 5.4 for the normal density bags. The additional bags used are presented in table A.2.

Three bag formation | Four bag diamond formation | Four bag stagger formation | Five bag dice formation

Figure 5.10: Pre-test photographs of evaluated group formations

The performance of the formations is classified based on top picture and video analysis as described in Section 5.2.

The most stable formations are the four bag diamond formation both head on and at a 45 degree angle and the three bag formation when waves approach head on. These formations increase stability with the same mechanism. The front bag, from the direction of the current, is partly lifted up on top of the middle bag or bags and so is less likely to roll over. The middle bag is supported by the others and the one in the rear is shielded by the front bag. In the three bag formation the bags are in a straight line

and it performs well when the waves approach head on. But when the waves are at a 45 degree angle the stability is lost. The four bag diamond formation performs much better at the 45 degree angle. In the four bag stagger, the bags at the edges of the formation are exposed and fail by moving out of the formation, resulting in less stability compared to the other ones. The five bag dice only worked when the centre bag was on top of the other bags. This formation does not outperform the other formations but requires one more bag.

	Wave condition				
Formation	1	2	3	4	5
3 bag	R	R	R	x	
4 bag diamond	R	R	S	R	x
4 bag stagger	x	R	x	x	
5 bag dice	R	R	x	x	
3 bag 45 degrees	x	x	x		
4 bag diamond 45 degrees	x	R	x	x	
4 bag stagger 45 degrees	R	S	x	x	

Table 5.3: Low density fill material grouped test comparison, x Indicates failure, S stable and R rocking.

	Wave condition						
Formation	1	2	3	4	5	6	7
3 bag	S	S	S	S	R	R	R
4 bag diamond		S	R	R	R	x	
4 bag stagger		x	R	x			x
5 bag dice		R	R	R	x		
3 bag 45 degrees	x	x					
4 bag diamond 45 degrees		R	R	x	R		x
4 bag stagger 45 degrees		x	R	x			

Table 5.4: 1 to 40 4 ton bag comparison of grouped formations. Regular wave conditions that cause failure for single bags of this type. x Indicates failure, S stable and R rocking.

The three bag and four bag diamond formations will be used in further analysis as these are the best performing formations. A comparison of the effectiveness of the formations to single rock bags is shown in Figure 5.11. One test is thrown out because the fitted wave is not correct for peak and trough and results in an untrustworthy orbital velocity amplitude, no failure occurred in this test. To reach failure for the normal density grouped bags, high energy waves are needed. These have high reflections. In 28 of 61 tests the combined velocity was determined to large compared to the fitted wave velocity to be trustworthy, so the fitted wave velocity was used. There is a probability that the velocities experienced by the formation temporarily exceeded the indicated velocity. In only a few cases failure was reached so this effect is difficult to account for.

In the considered head-on tests the four bag diamond formations are stable at more than 1.5 times the single bag limit as is suggested in other work. For the three bag formation there is only one failure below 1.5 times the single bag limit, by a low density bag. Since the normal density tests do not reach failure, this might not be representative. In the tests with a 45 degree angle both formations perform worse. As is displayed in tables 5.3 and 5.4. The four bag formation has higher stability in this case, if the three bag formation outperforms a single bag in this case can be doubted. A grouping factor K_g is proposed for the stability equation, with $1 < K_g \leq 1.5$.

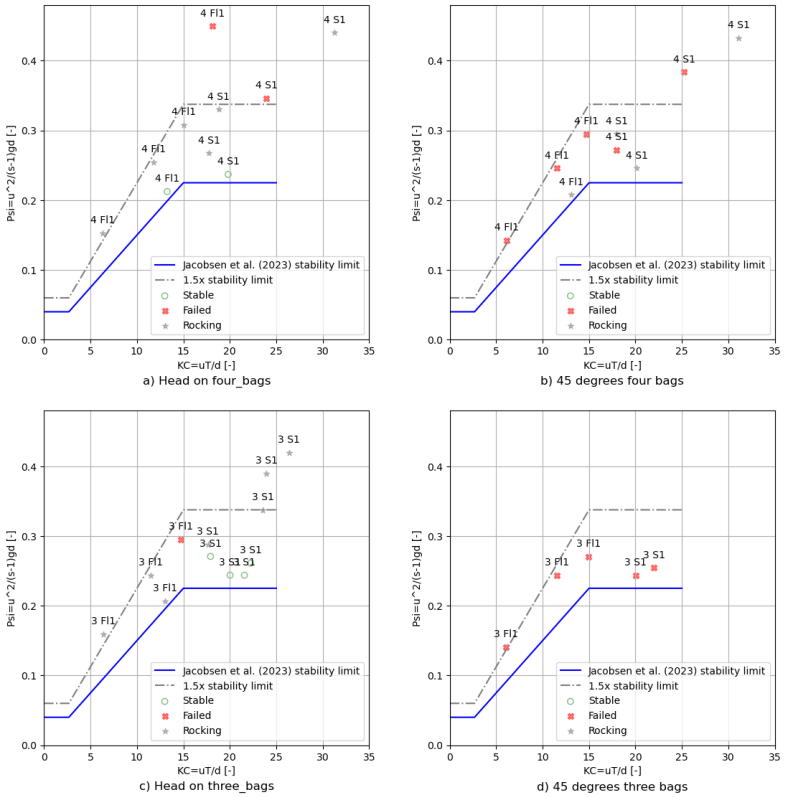

Figure 5.11: Scatter plot of the results of 3 bag row and 4 bag diamond formations. Compared to the extended Jacobsen et al. (2023) stability limit and 1.5x that limit.

5.5. Irregular wave tests

In this section the results of irregular wave tests are discussed. The method for the analysis of irregular wave data can be found in appendix D. Rock bags do not fail by gradual displacement, but rather one or more large displacements. This movement is thought to be dependent on the larger waves in a spectrum. Orbital velocities calculated with linear wave theory from the surface elevation data are used for the analysis. When using the two percent exceedance probability wave height $H_{2\%}$ in the analysis, the stability limit matches the limit obtained from regular wave tests. In these experiments, at least 20 waves exceed the 2% wave height, so the number of waves is comparable to that of regular wave tests. The distinction is that in regular wave fields, these waves are in direct succession, while for irregular wave fields this is not the case. Due to interference of spectral components larger waves are expected to occur in groups of a number of large waves in a row, depending on the spectral shape. The analysis of measured orbital velocities is elaborated on in Section D.2.2. The maximum wave height is limited by the water depth. This limit can be seen as levelling off in the Rayleigh distributions, see Figure D.11.

The results of irregular wave tests for single rock bags on a rough bed can be found in Figure 5.12. If all tests are considered the extended stability limit seems to give an accurate prediction for the onset of failure conditions. No failures and limited rocking is observed below the limit. There is however, some uncertainty as there are many stable or rocking tests results above the limit. None of the tested 1 to 30 scale bags failed, but most are classified as rocking above the limit. For the small fill material bags a single failure occurred. These are the main rock bags for this research, as they are used for the grouped and full model tests. Thus, it might be possible for stable conditions to exist beyond this limit. A difference for the comparison of large and small fill material is observed in the irregular wave tests, when compared to the regular wave tests. Although there are fewer data points from these tests, see Figure 5.12. The wide-graded bags are most stable in those experiments and the large fill material bags are the least stable. This suggest there is a negative influence of the porous flow on the stability as suggested by Coghlan et al. (2024). The porous flow is largest for the large fill material and smallest for the wide graded material. The theoretical bulk density of the wide graded material is larger due to

the lower porosity, this could also have a positive effect, see chapter 2.

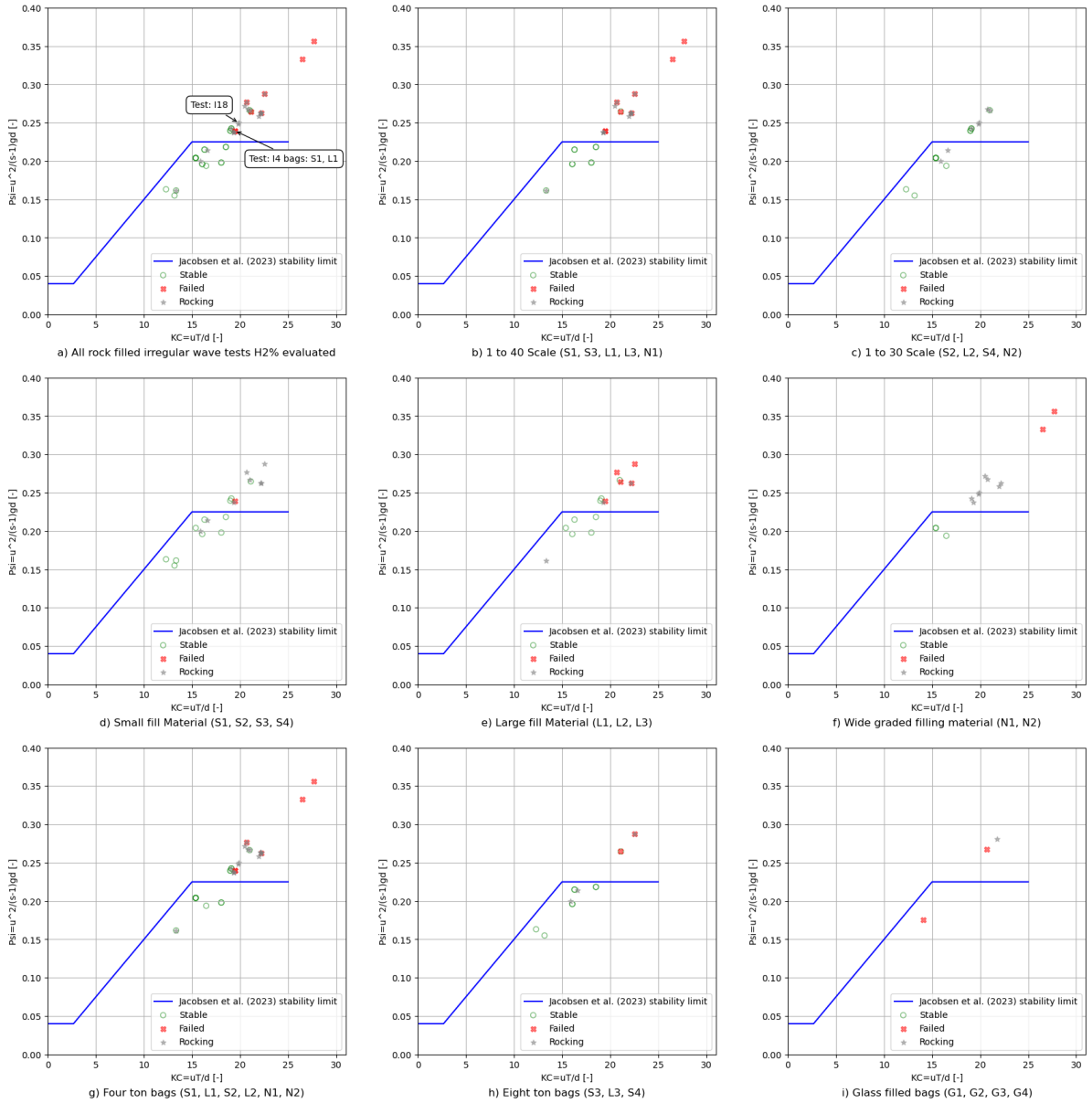

Figure 5.12: Results of irregular wave tests with normal density bags compared to the Jacobsen et al. (2023) stability limit. Orbital velocity amplitudes computed with the 2% exceedance probability wave height.

5.5.1. Irregular full model tests

The tests are done in the set-up as described in chapter 4. The bag is placed with its edge on the touchdown point of the CPS model. Approximately $0.5D_{pile}$ from the edge of the monopile. For formations the edge of the farthest inward bag is placed on the touchdown point. In table 5.5 the-range of rock bag-diameters compared to the 250 mm pile diameter.

In most tests there are quite some reflections of waves against the pile, these seem to interact with the incoming waves, but not close to or behind the pile. The pattern of reflections is semi circular. Some waves follow the shape of the pile and then reflect of the back wall. In wave troughs there is an outpour of water from the half pile that also causes small surface waves, these are not expected to have an impact on bottom orbital velocities. If the pile had been glued to the back wall this could have been prevented. In some tests the pile itself also shakes or is lifted slightly. In the tests with a lower water level and with long waves, there are upward forces on the CPS model.

When a single rock bag serves as the CPS stabilization, the CPS exerts the critical force on the bag. In

Bag	Scale	Diameter [mm]	Ratio D_{bag}/D_{pile}
S1 4 ton	1:40	60	0.24
S2 4 ton	1:30	80	0.32
S3 8 ton	1:40	75	0.3
S4 8 ton	1:30	100	0.4

Table 5.5: Comparison of rock bag and pile diameters at different model scales, pile diameter of 250 mm

these tests the cable is forced and pushes the bag, but the bag itself is not rotating or rocking. In 14/20 (70%) failures of a single bag, the cause of failure was deemed to be the force exerted on the bag by the CPS. In some tests the internal motion of the fill material, motion of the bag and force of the cable combined led to failure level reshaping. The [effective] weight of the CPS relative to the bag is thought to be important. The same CPS is used for 1 to 30 and 1 to 40 scale tests. So, the relative weight is greater and the relative diameter bigger on 1 to 40 scale. This could result in lower stability for the 1 to 40 scale. For grouped bags force by the CPS is only in one case the cause of failure. Mostly, stability of the vulnerable front bag is critical for failure. In the 75 degree case the front bag gets pushed towards the monopile.

In Figure 5.13 the resulting scatter plots of the tests are shown. 90 and 75 degrees are the most critical for both grouped and single bags. In the 105-degree tests the bags are more stable, also in direct comparison with the same condition.
The amplification factor for the flow at the location of the rock bag is between 1.2 and 1.5 according to potential flow theory and Schiereck and Verhagen (2019), see Section 2.3. This flow amplification is responsible for part of the decrease in stability. The decrease in stability is not observed for the lower KC numbers. This could be due to the influence of turbulence development around the monopile. So, it is suggested to not lower the stability limit in this region, but only from the level of onset of instability. An average amplification factor of 1.35 is suggested. This is squared with the velocity to find the reduced critical value. Below the KC this line intersects with the rough bed limit is thought to be adequate. The adapted limit is described as a stability factor K_{pile} multiplied with ψ_{cr}, this limit is shown in Figure 5.13:

$$\frac{u_{2\%}^2}{(s-1)gD_{rb}} < K_{pile}\psi_{cr} = \begin{cases} 0.04 & \text{if } KC < 2.67 \\ 0.015 \cdot KC & \text{if } 2.67 \leq KC \leq 8.2 \\ 0.123 & \text{if } KC > 8.2 \end{cases} \tag{5.1}$$

It should be noted that the value of KC is calculated with the $u_{2\%,0}$ orbital velocity, so without the influence of the amplification. This is because the amplification factor results in a small difference for the position on the KC axis and this will predict higher stability by moving the points further from the sloped part of the stability limit.

Alternatively, the loss of stability can be expressed by a flow amplification factor K_v, that is used to obtain a single stability equation for all cases.

$$\frac{(K_v u_{2\%})^2}{(s-1)gD_{rb}} < \psi_{cr} = \begin{cases} 0.04 & \text{if } KC < 2.67 \\ 0.015 \cdot KC & \text{if } 2.67 \leq KC \leq 15 \\ 0.225 & \text{if } 15 \leq KC \leq 25 \end{cases} \tag{5.2}$$

With:

$$K_v = \begin{cases} 1 & \text{if } KC < 8.2 \\ \sqrt{0.122 \cdot KC} & \text{if } 8.2 \leq KC < 15 \\ 1.35 & \text{if } KC \geq 15 \end{cases} \tag{5.3}$$

The newly obtained limit can be multiplied by the suggested factor K_g to determine a limit for grouped bags. Figure 5.13 shows that all grouped formation tests that failed exceeded this combined limit value. Because of the small number of grouped tests, particularly near the limit, it is impossible to accurately assess stability. Because of this, the combination of the grouping factor K_g from Section 5.4 and the flow amplification factor from this section should not be taken at face value without further research. It could rather serve as a hypothesis for future investigation and model testing.

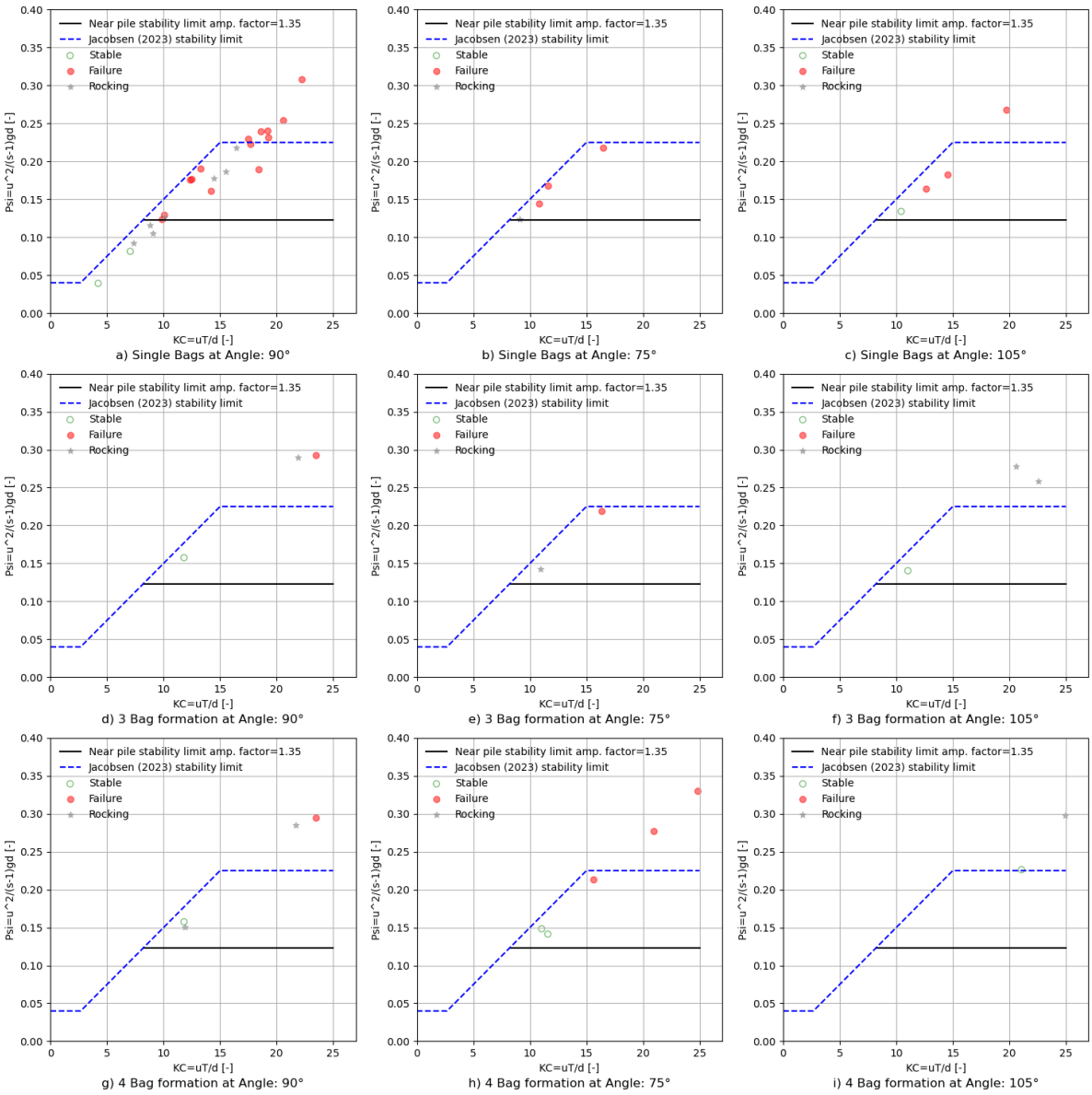

Figure 5.13: Results of irregular wave tests near the monopile compared to the Jacobsen et al. (2023) stability limit. Orbital velocity amplitudes computed with the 2% wave height. Flow amplification factor of 1.35 is implemented for $KC > 8.2$ for the new stability limit of $\psi_{cr} = 0.225/1.35^2 = 0.123$.

5.5.2. Influence of the CPS

Some test are conducted with hollow cable as CPS model. With this low weight cable (near 0 effective weight), the bags failed in all cases due to movement of the CPS. For the same conditions with the normal weight CPS model, the bags remained stable for a longer time, but eventually also failed. In two cases due to the cable, but one time due to the normal rolling failure mechanism of the bag.
A number of tests were conducted without a CPS model. The results can be seen in Figure 5.14. There are too few data points to draw a conclusion other than that there is no failure below the proposed limit, but that there is-failure in many cases lower than the open water limit. It is possible that the near pile limit is too conservative for the case without a CPS, as in the experiments with a CPS most bags seem to have failed due to force exerted on the CPS. However, from these tests this conclusion cannot be reached. In the experiments classified as failure, there was no doubt about the classification as the bags clearly failed by the normal mechanism.

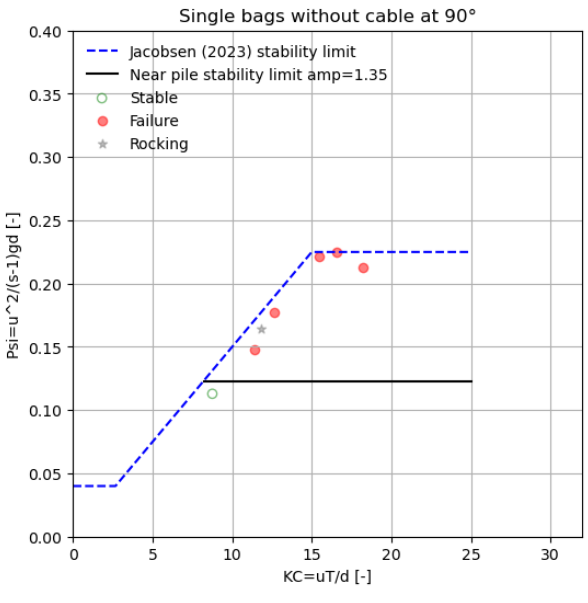

Figure 5.14: Results of irregular wave tests for single bags without a CPS at 90°, compared to the stability limits. Orbital velocity amplitudes computed with the 2% wave height. Flow amplification factor of 1.35 is implemented for $KC > 8.2$ for the new stability limit of $\psi_{cr} = 0.225/1.35^2 = 0.123$.

5.6. Combined wave current

Typically, design conditions include a combination of wave and current. Both regular and irregular wave conditions are tested in combination with a steady current. Due to the difficulties associated with reflections and interference patterns in analysis, only the results from irregular wave-current tests are considered.

For the tested range of steady currents, there is visually little difference in the stability of rock bags in the full model, see Figure 5.15. However, there is a new observed failure mechanism for grouped bags and CPS: Sliding of the entire formation. The current is thought to cause an additional drag force on both the cable and bag. In the videos gradual displacement by small increments in the direction of the current can be seen during positive orbital velocities. This can cause enough displacement for the test to be classified as failure. Since the bags themselves do not show the rocking type failure mechanism, this sliding failure is thought to be the result of the drag force on both the bag and cable. So the drag force is more important compared to the inertia in these cases.

For all considered currents, use of only the wave orbital velocity in the calculation is a good predictor of stability, see Figure 5.15. Most tests are done with approximately the same velocity, except for two. The one with maximum current failed, but failure due to only the wave forcing could have been expected. The one test with low velocity was stable, but that would also be expected based on only the waves. For near bed h=10 cm, velocity in a range of $0.1 < u < 0.15$ m/s at model scale, the failure due to combined wave-current conditions is well represented by the wave-only calculation of stability. These steady current velocities were up to 45% of the 2% exceedance probability orbital velocity amplitude.

The method that Jacobsen et al. (2023) suggested for assessing stability in a combined wave-current condition was not based on tests with combined conditions. Based on the present results, that method is not found to accurately predict the stability in the tested combined wave-current conditions. Analysis does indicate that better results might be obtained with the use of a stability limit based on addition of wave and current induced shear stresses.

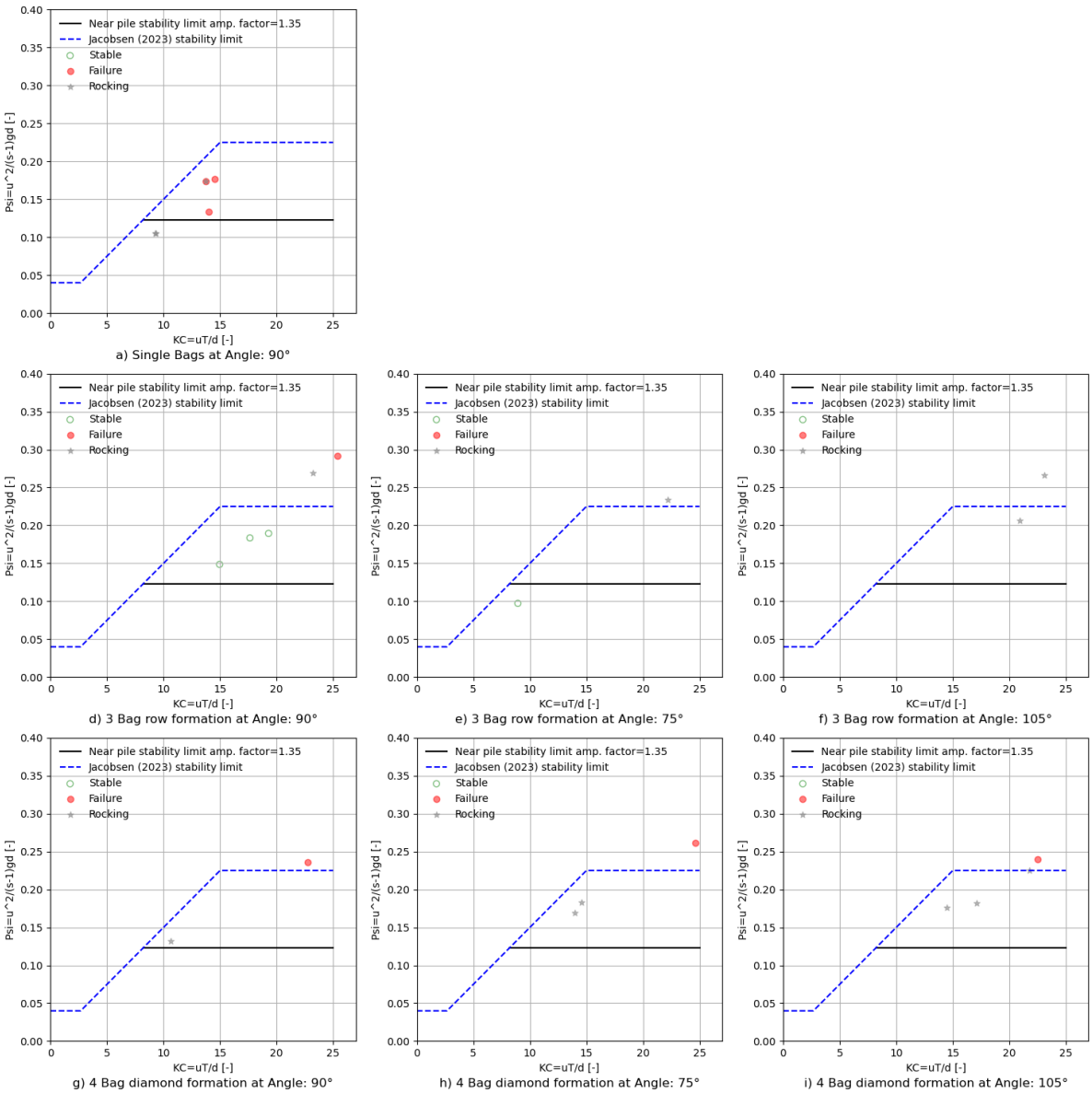

Figure 5.15: Results of irregular wave tests with combined current conditions. Stability numbers are calculated with only the wave orbital velocities computed with the 2% wave height. These are a good predictor for the stability when compared to the stability limit presented in this chapter. Stable conditions for steady currents up to 45% of the 2% orbital velocity amplitude

5.7. Slope tests

In this section the results of slope stability tests for the rock bags are discussed. These experiments give insight in the differences between the bag types.

A total of 304 slope tests have been conducted, to find the angle of response for rock bags on varying surfaces. The tests were conducted by placing a bag on a plank covered with smooth wood, sandpaper of glued rocks. On the sandpaper and rock covered slopes the bags failed by rolling down, while on the smooth surface only sliding was seen. This sliding failure started at much smaller angles for all types compared to the rolling. The plank is lifted on one side to increase the slope. The angle is visually tracked along a protractor made for these experiment. The slope is increased until failure is reached. The angle where movement starts to occur is recorded. For each bag this is repeated three times for all surfaces.

In table 5.6, the results are shown. All rock filled bags had relatively similar angles of response. The low internal friction glass spheres filled bags failed at the smallest angles for all tests. The relatively

rigid, low density bags failed at the largest angle averaged for the three surfaces. This confirms the hypothesis that more rigid bags with higher internal friction are more resistant to rolling failure than those with low internal friction.

Number of bags and type	Smooth bed [degrees]	Sandpaper bed [degrees]	Rough bed (glued Rocks) [degrees]
30; Average	22	54	48
12; Small narrow graded S	22	56	48
4; Large narrow graded L	22	56	47
2; Wide graded N	23	53	46
4; Glass G	20	49	43
4; Low Density	22	56	50
5; Test bags	22	54	48

Table 5.6: Angle of failure for rock bags on a gradually increasing slope for the indicated surface of the slope.

6

Discussion

Waves and data analysis

This was the first experimental campaign using a new wave maker and flume setup. As a result, it was not fully known what could and could not be done with the set-up. The wave maker performed well, as it was able to generate the requested very large non-linear regular waves. In retrospect, the scale of the experiments necessitated waves that approached the limit of the set-up. The parabolic dampener was unable to completely absorb these extremely high regular waves, which caused reflections. The dampener was not designed for these types of waves, and it was raised to allow current to flow underneath.

The wave height gauges were placed in the centre between wave maker and set-up to cause as little disturbance as possible and allow for the two EMS' in between. These were placed far apart to be able to detect non-developed flow. Due to this positioning and the standing interference pattern between incoming and reflected regular waves, it proved difficult to make an accurate assessment of the actual wave height and orbital velocity at the model set-up.

The thin probes of the measurement devices cause only minor disturbances. As a result, a better approach would have been to place the wave height gauges and EMS' closer to the setup and in a single array. In this case, the measured orbital velocities and wave heights can be precisely compared. For both regular and irregular wave tests, the measured orbital velocities differ from those calculated.

In regular wave analysis, fifth order wave theory is used to compute orbital velocities, taking into account the incoming and reflected signals. There are large differences between measured and calculated velocities. This could be because the harmonic does not accurately describe the reflected signal, or there are differences between expected and actual spatial interference patterns. It's also possible that the EMS doesn't capture the full velocity signal.

Regular wave stability analysis uses either the maximum combined incoming and reflected wave velocity amplitude or the incoming fitted wave orbital velocity amplitude. The latter is used when the combined velocity amplitude at the model setup is less than the incoming signal, which is not the case in the first few waves. This implies that the velocity was present at the set-up, albeit possibly for a shorter period. The fitted wave velocity is also used when an arbitrary limit of 15% increase in velocity by the reflected wave is exceeded. This was done because such an increase is considered unrealistic over the entire test. In several tests where such an increase was calculated, the rock bags would then have been stable far beyond the limit.

In the irregular wave analysis orbital velocities are calculated based on linear wave theory. There is a constant difference in the m0 component of the calculated and measured velocity of around 23%. For less non-linear wave fields the difference in 2% exceedance probability velocities is smaller than the difference for the m0 component. For wave fields that are more non-linear the difference is similar to that of the m0 velocity. It is unclear whether this difference is due to the calculations, the measurements, or both.

Regular and irregular wave tests produced high reflections, with an average reflection coefficient of 0.27 for regular wave tests and in the range 0.07 to 0.44. The parabolic dampener buckled due to

the waves. It couldn't be placed at the end of the flume, so it was placed a few meters ahead to keep splashes of breaking waves from damaging wiring. This allowed reflecting waves to travel back and forth between the dampener and the back of the flume, interacting with incoming waves on the dampener and reducing its effectiveness.
Higher order waves appear in the troughs of highly nonlinear regular waves, because the wave maker theory is not suited for the non-linearity depth. To prevent the generation of these waves a transition slope could have been used (Eldrup and Andersen, 2024), although this would have been difficult to fit in the flume and depth would further be reduced. Another possibility would be the use of Cnoidal wave maker theory.

CPS and monopile

In monopile tests, the interaction between the pile and water was not always flawless. The pile was not glued to the side wall. As a result there was out pour of water in the wave troughs and the pile shook or was lifted occasionally. Very little information was available on the parameters of a CPS, so scaling was difficult. Therefore, it is not known how the weight and stiffness of the used model CPS compares to prototype scale. The effect of these parameters on the forces excerpted on the bags by the CPS is also not known.
The CPS appeared to exert a force on the rock bags, influencing their stability. When rock bags were tested in combination with the monopile but without a CPS, no notable increase in stability was observed. The CPS' force might only trigger failure when the rock bags are close to failure due to the overturning mechanism and the bag starts to lose contact with the bed. This suggests that most failures would occur with or without CPS.

Stability limit

Inertia is not taken into account in the stability limit, while this is found to be an important component, as for steady current much larger critical flow velocities are observed compared to the critical orbital velocities. There is a stability gain at larger KC numbers, this is due to the decrease in relative accelerations. Jacobsen et al. (2023) hypothesized that the stability became constant for KC>15, which seems to be confirmed by the present tests for the range $15 < KC < 25$.

In the method for evaluating stability the period, orbital velocity and rock bag diameter influence both the ψ and KC values. The maximum steepness of waves and density of the material determine the envelope of possible points in the plot and the KC interval where the limit can be exceeded. For high density material the waves that will cause failure might exceed the critical value at higher KC. From the present experiments no conclusion about an increase of the stability limit above $KC = 25$ can be drawn.

In regular wave tests, the stability limit serves as a lower bound for the onset of instability. There are numerous stable points above the limit. This is especially true for larger rock bags. This may also be related to the highly nonlinear waves required to move these bags in this facility. The period of the maximum amplitude velocity in these waves is shorter than the linear period.

All irregular wave fields had the same spectral shape. It is not be known if the coupling between the 2% exceedance components, the peak period and the limit also holds for very different spectral shapes. If for example the wave grouping is different and the probability of the highest waves having the peak period is lower. Since most storms have similar spectra and the influence of low and high frequency components is limited this should not be of large concern. It should only be considered for spectra that differ considerably from the average JONSWAP.

The irregular wave current tests indicated that the current had little influence on stability near the monopile. The tested range with stable results includes current velocities up to 45% of the 2% exceedance probability orbital velocity amplitude. However, most tests were performed with similar current so it is unclear up to what steady current velocity this may be true. Unfortunately, it was decided to not include the results of regular wave combined current tests due to the time limitations on the project and difficulties in analysis.

Scaling effects

Larger bags than the eight ton were not tested. It is not clear if the gain in stability proportional to the diameter will increase for larger rock bags. The 8 ton bags at both scales performed very well, with only a few failures beyond the limit in the regular wave tests, so there is little indication that the relation does not hold at larger sizes.
During the monopile tests, the eight ton bags performed comparable to the four ton bags, for similar stability parameters. There is a difference in the observed effect of fill material and porosity between irregular and regular wave tests. These parameters have little effect on stability in regular wave tests but there are some differences in irregular wave tests. The reason for this is not known.

The size of the fill material at the model scale was determined by adjusting the Froude scaled size to achieve equal mobility with the prototype scale material. The first level of movement observed in model rock bags was that of internal material. Mobility scaling is thought to be important for accurately representing this movement. The gradual movement of internal material did not result in failure in these experiments. This is also to be expected at prototype scale, because fill material has equal mobility at model scale. This scaling method increases the size of the fill material at model size, which helps to reduce the scale effects of porosity and internal friction.

In regular wave tests the varied porosity of the fill material seemed to cause little difference. In irregular waves the results were different, but this included much less tests and little direct comparison. The difference between the small material bags (S) and wide graded material bags (N) was not pronounced. Adapting the porosity of the material changes the bulk density of the rock bag. The difference in bulk density between the wide and narrow graded material: $(1 - n_{wide})/(1 - n_{narrow}) = 0.6/0.54 = 1.11$. This is not considered in the current definition of the stability limit, where the volume of rock is used.

The scale effect that introduces most uncertainty is the internal friction. From the tests with glass filled bags it can be concluded that it is an important parameter. The extreme lack of internal friction between these glass spheres means that the friction at prototype scale is likely larger. For now the magnitude at prototype scale is not known. It could also be dependent on the material used, as the friction between more squared rocks with sharp edges is expected to be larger compared to round boulders. The glass bags were less stable compared to the other model bags. A reduction factor of 0.75 is found for the least stable variant with very small spheres (G1) and 0.82 for the others.

7

Conclusion

The research leads to the conclusions presented in this chapter. In Section 1.3 a main research question was formulated based on six sub-questions. First, an answer will be given to each of these sub-questions, followed by a final answer to the main question.

1. *How do rock bags respond in offshore wave loading, what are the observed motions and failure mechanisms?*

   Four levels of movement are observed during the tests: local internal material movement, partial bag uplift, rocking of the entire bag, and overturning. Model rock bags filled with normal density material placed on a rough bed failed due to a rocking like motion that caused rotational movement around a part of the bag that is in contact with the bed. This could result in complete overturning. A similar failure mechanism at a lower load was observed for rock bags filled with glass spheres.

2. *Which properties of rock bags influence stability, and how can their influence be quantified?*

   The resistance of a rock bag to the hydraulic forces responsible for the failure mechanism is determined by the diameter of the rock bag and the relative density of fill material.

   The internal friction of the fill material also has a role in the failure mechanism of the rock bag and the load at which it occurs. The bags filled with glass spheres with low friction showed the same failure mechanism as the rock filled ones, whereas the high friction low density fill material bags showed a more rigid body overturning failure. In the slope stability tests, the glass material bags were least stable and the stiff low density bags were most stable, likely due to the internal friction. As the glass filled bags are a limit case for extremely low internal friction and these show the same failure mechanism as the rock material filled model bags, this is considered the representative mechanism for bags filled with material with internal friction levels in between. This range likely includes prototype rock bags. It is suggested to include a factor in the stability limit to account for the uncertainty about the scale effect of internal friction. With a minimum value equal to the difference between the stability limit of low friction glass fill material and rock fill: $0.75 \leq K_{fr} \leq 1$.

   In regular wave test the size of the fill material did not cause large differences in stability for the tested range: $2.9\% < d_{50}/D_{bag} < 4.7\%$. For irregular waves there was a difference. Bags filled with larger material than specified by the manufacturer are more likely to fail in conditions exceeding the stability limit.

   From regular wave tests little difference was observed for the stability of wide or narrowly graded filling material, in the irregular wave tests the wide graded fill material was more stable in conditions exceeding the stability limit.

3. *What is the limit for stability that can be derived from the experiments, and how does this compare to the literature?*

A failure criterion is developed based on analysis of before and after top pictures of the tests. Bags that are displaced by more than 1/6th of their diameter, approximately equal to a CPS diameter, are classified as failed; with less displacement classified as rocking; and with only local changes of the shape or no differences as stable. This corresponds to the observed levels of movement.

The Jacobsen et al. (2023) stability limit was based on empirical results up to $KC = 15$ and an extension of the limit for larger KC values was hypothesised. In their study the classification was based on visual observation during. The regular wave results from the present study are compared to the limit, with orbital velocities computed from fifth-order wave theory. The extended limit is valid as a lower bound for the occurrence of mobility, with 69/72=95.8% of failures above the limit and 128/144=88,9% of non-stable (failure and rocking) conditions.

4. *What is the stability in an irregular wave field, and which wave statistic most accurately quantifies it?*

   If an irregular wave field is evaluated with orbital velocities calculated with linear wave theory for the 2% probability of exceedance wave at peak period $u_{2\%}$, the same limit is a good predictor for the lower bound for the occurrence of failure for the open water rough bed case. All conditions with failure are above the limit and 24/27=88,9% of non-stable test conditions are above. Stability is also observed above the limit as 6/22=27% of stable conditions are above. The stability limit:

$$\frac{u_{2\%}^2}{(s-1)gD_{rb}} < \psi_{cr} = \begin{cases} 0.04 & \text{if } KC < 2.67 \\ 0.015 \cdot KC & \text{if } 2.67 \leq KC < 15 \\ 0.225 & \text{if } 15 \leq KC \leq 25 \end{cases} \tag{7.1}$$

   $KC = \frac{u_{2\%} T_p}{D_{rb}}$, with T_p the peak period, D_{rb} the diameter of the rock bag and $s = \frac{\rho_s}{\rho_w}$ the ratio of rock and water densities.

5. *What is the influence of grouping or stacking multiple rock bags on stability, considering formations applicable to CPS stabilization?*

   Out of four evaluated grouped formations the four bag diamond performed best in the rough bed and CPS stabilisation tests. In these cases the formation increases the stability limit considerably. A factor K_g can be multiplied with ψ_{cr} to express this gain in stability due to grouping. From the results of this study the factor is proposed as $1 < K_g < 1.5$, where 1.5 can be used for head on direction.

   The three bag row formation also performed well when the waves approached head-on, but did not increase the stability for waves from a 45 degree angle. In the CPS stabilisation it performed similar to the four bag diamond.

6. *What is the stability of rock bags when applied in a CPS stabilization application near a monopile foundation and what is their performance in stabilizing the CPS?*

   When a single rock bag is used in the CPS stabilisation role in 14/20 failures the cause was deemed to be the force exerted on the bag by the CPS. For both grouped and single bags the most critical angles for stability around a monopile in the CPS stabilisation role were 75 and 90 degrees from the wave incidence. Higher stability was observed at 105 degrees.

   When a flow amplification factor K_v is used, an accurate prediction for the lower bound for the occurrence of failure of a single rock bag near a monopile is found. All failed conditions exceed the limit and 18/21=85.6% of non-stable conditions are above the limit for the 90 degree case with CPS. For the 75 and 105 degree cases with CPS all non-stable conditions are above this limit. This is also true for tests with a single rock bag near the monopile without a CPS. The flow amplification factor is defined as:

$$K_v = \begin{cases} 1 & \text{if } KC < 8.2 \\ \sqrt{0.122 \cdot KC} & \text{if } 8.2 \leq KC < 15 \\ 1.35 & \text{if } KC \geq 15 \end{cases} \tag{7.2}$$

Where KC is calculated with the $u_{2\%,0}$ orbital velocity, so without the influence of the amplification. Both considered formations for grouping have higher stability compared to single bags for all angles and conditions tested. The increase in stability could be equal to the increase observed for rough bed tests K_g as no formations failed for $\frac{(K_v u_{2\%})^2}{(s-1)gD_{rb}} < K_g\psi$, However, there is a high level of uncertainty because a limited number of tests were performed with formations in the full model, so this combination cannot be used without further verification.

What is the hydraulic stability of rock bags under wave loading in offshore application for the stabilisation of CPS.

In this research the hypothesised extended limit by Jacobsen et al. (2023) has been used to describe the stability. The limit is defined for the orbital velocity calculated from linear wave theory using the 2% exceedance probability wave height and peak period. Flow amplification around a monopile can reduce the stability. Grouping of the rock bags was found to have a positive effect on stability. The loads transferred by the CPS to the rock bag need to be considered as these might have a negative impact on stability. The answer to the main question of this research is given in the form of the full equation for stability:

$$\frac{(K_v u_{2\%})^2}{(s-1)gD_{rb}} < K_g K_{fr} \psi_{cr}, \quad \psi_{cr} = \begin{cases} 0.04 & \text{if } KC < 2.67 \\ 0.015 \cdot KC & \text{if } 2.67 \leq KC < 15 \\ 0.225 & \text{if } 15 \leq KC \leq 25 \end{cases} \tag{7.3}$$

For $KC = \frac{u_{2\%} T_p}{D_{rb}}$, with T_p the peak period and D_{rb} the diameter of the rock bag. $s = \frac{\rho_s}{\rho_w}$ is the ratio of rock and water densities and $g = 9.81 m/s^2$ the gravitational acceleration. K_g the grouping factor, K_{fr} the factor representative for the uncertainty on internal friction at model scale and K_v the flow amplification factor.

8

Recommendations

The following recommendations are made for future research and the interpretation of the results of this study for the use of rock bags.

- Because of the unresolved scale effect of internal friction, the limit found in this study may not be applicable to prototype scale bags, therefor the use of K_{fr} is suggested. Large-scale rock bag tests can help to resolve this issue. There are multiple large flume facilities available in the world. In these facilities it may be possible to test four ton bags up to a scale of $\approx$ 1:5. This can be combined with a repeat of the slope tests performed in this study, by using a flat bed truck to create a smooth slope. The rolling resistance on a rough slope is more informative, but likely more difficult to recreate at larger scale.
- In this research only rock bags placed in the streamline contraction zone of the flow around a monopile were evaluated, as these are the angles with maximum drag force on the CPS. The stability of rock bags placed in the wake or on the upstream side needs to be determined. Lower stability might also result from the turbulence that lee-wake vortexes and the horseshoe vortex produce.
- The rock bags were placed on the touchdown point of the CPS at approximately 1 pile radius from the monopile. The exact position can have a major influence on stability, as the flow amplification depends on the distance from the pile. For the use of the stability limit it should be noted that the K_v factor is not applicable for bags placed at a much different location.
- The effect of rock bags placed on a reshaping scour protection is to be evaluated. The turbulence generated by the rock bag might cause edge scour, which could threaten the stability of the rock bag as described by Riezebos et al. (2021).
- A new method has to be developed to be able to determine the stability in a combined wave-current condition, beyond the current velocities used in this experiment. It is recommended to include the inertia of the oscillatory orbital velocities in this method.
- Further investigation is needed to examine how the design of the CPS impacts stability. Particularly, the stiffness and density of the CPS will impact both the stability of the system and the force exerted by the CPS on the rock bag. These forces should be considered in design studies. Other failure mechanisms for combined failure must also be considered, such as the CPS being pulled out from under the rock bag, these were not observed in this study.
- Additional research is required to assess the effectiveness of stabilisation in preventing damage to the CPS. The remaining free span may cause movement or vibration in the CPS. The resulting stresses on the stabilised CPS should be considered in the design of stabilised rock bag systems.
- It is possible to change the shape of the bag. In this study, the manufacturer's suggested shape was assumed. It is unclear whether this is the optimal shape, so an altered shape may improve performance.
- Additional research can be done for the effect of the spectral shape on the stability in irregular wave fields and the use of $H_{2\%}$ combined with the peak period T_p. This is likely only of concern for design conditions with spectra that differ fundamentally from the JONSWAP spectra, for example a spectrum with multiple peaks.

References

Bluemont. (2024). Kyowa rock bags: Natural protection for the enviroment [https://www.bluemont.com.au/erosion/kyowa-rock-filter-bags/].

Brouwers, H. (2023). Random packing fraction of binary similar particles: Onsager's model revisited. *Physics-Uspekhi*, *67*. https://doi.org/10.3367/UFNe.2023.11.039606

CIRIA. (2007). *The rock manual: The use of rock in hydraulic engineering* (2nd).

Cirtex. (2023). Rock bags: Technical data sheet [https://cirtexcivil.co.nz/products/rock-bags/cirtex-rock-bags/].

Coghlan, I., Carley, J., & Messiter, D. (2024). Physical modelling of rock bags under wave attack. *Proceedings of the 9th International Conference on Physical Modelling in Coastal Engineering (Coastlab24)*. https://doi.org/10.59490/coastlab.2024.703

Dixen, M., Hatipoglu, F., Sumer, B. M., & Fredsøe, J. (2008). Wave boundary layer over a stone-covered bed. *Coastal Engineering*, *55*(1), 1–20. https://doi.org/https://doi.org/10.1016/j.coastaleng.2007.06.005

Durakovic, A., & Offshorewind.biz. (2022). Ørsted expects much lower hit from cable protection system issues than anticipated. *Offshore Wind*. https://www.offshorewind.biz/2022/04/29/orsted-expects-much-lower-hit-from-cable-protection-system-issues-than-anticipated/.

Ehlers, W. (2022). Darcy, forchheimer, brinkman and richards: Classical hydromechanical equations and their significance in the light of the tpm. *Archive of Applied Mechanics*, *92*, 619–639. https://doi.org/10.1007/s00419-020-01802-3

Eldrup, M. R., & Andersen, T. L. (2024). Generation of highly nonlinear waves in a short wave flume. *Proceedings of the 9th International Conference on Physical Modelling in Coastal Engineering (Coastlab24)*. https://doi.org/10.59490/coastlab.2024.68

Fenton, J. D. (1985). A fifth-order stokes theory for steady waves. *Journal of Waterway, Port, Coastal, and Ocean Engineering*, *111*, 216–234.

Fenton, J. D., & McKee, W. D. (1990). On calculating the lengths of water waves. *Coastal Engineering*, *14*, 499–513.

Fenton, J. (1990). Nonlinear wave theories. *Ocean Engineering Science*, *9*.

Gupta, B. K., & Basu, D. (2020). Offshore wind turbine monopile foundations: Design perspectives. *Ocean Engineering*, *213*, 107514. https://doi.org/https://doi.org/10.1016/j.oceaneng.2020.107514

Herdayanditya, I., Streichers, M., Lataire, E., & Rauwoens, P. (2024). Experimental study of irregular wave field with moderate steepness around a monopile. *Proceedings of the 9th International Conference on Physical Modelling in Coastal Engineering (Coastlab24)*. https://doi.org/10.59490/coastlab.2024.686

Hofland, B. (2005). *Rock and roll. turbulence-induced damage to granular bed protections* [Dissertation (TU Delft)]. Delft University of Technology. FEBO Druk B.V.

Holthuijsen, L. H. (2007). *Waves in oceanic and coastal waters*. Cambridge University Press. https://app.knovel.com/hotlink/toc/id:kpWOCW0002/waves-in-oceanic-coastal/waves-in-oceanic-coastal

Jacobsen, N. G., Barrera, N. N., Giarrusso, C., & Christensen, E. D. (2023). Stability of rock-filled mesh bags. In T. U. Petersen & S. Sassa (Eds.), *Proceedings of the 11th international conference on scour and erosion*.

Jensen, B., Jacobsen, N. G., & Christensen, E. D. (2014). Investigations on the porous media equations and resistance coefficients for coastal structures. *Coastal Engineering*, *84*, 56–72. https://doi.org/https://doi.org/10.1016/j.coastaleng.2013.11.004

Lara, J. L., Losada, I. J., Maza, M., & Guanche, R. (2011). Breaking solitary wave evolution over a porous underwater step. *Coastal Engineering*, *58*(9), 837–850. https://doi.org/https://doi.org/10.1016/j.coastaleng.2011.05.008

Losada, I. J., Lara, J. L., & del Jesus, M. (2016). Modeling the interaction of water waves with porous coastal structures. *Journal of Waterway, Port, Coastal, and Ocean Engineering*, *142*(6), 03116003. https://doi.org/10.1061/(ASCE)WW.1943-5460.0000361

Ma, L. (2020). Stokes wave computationand fitting method [Open-source repository].

Maxey, M. R., & Riley, J. J. (1983). Equation of motion for a small rigid sphere in a nonuniform flow. *The Physics of Fluids*, *26*(4), 883–889. https://doi.org/10.1063/1.864230

Melville, B. W., & Raudkivi, A. J. (1977). Flow characteristics in local scour at bridge piers. *Journal of Hydraulic Research*, *15*, 373–380. https://api.semanticscholar.org/CorpusID:120800765

Miles, J., Martin, T., & Goddard, L. (2017). Current and wave effects around windfarm monopile foundations. *Coastal Engineering*, *121*, 167–178. https://doi.org/10.1016/j.coastaleng.2017.01.003

Petersen, T. U., Sumer, B. M., Fredsøe, J., Raaijmakers, T. C., & Schouten, J.-J. (2015). Edge scour at scour protections around piles in the marine environment - laboratory and field investigation. *Coastal Engineering*, *106*, 42–72. https://doi.org/10.1016/j.coastaleng.2015.08.007

Ridgeway. (2024). Kyowa's filter unit: For offshore wind farm, oil and gas market. japanese technology [https://rockbags.com/tag/ridgeway-marine/].

Riezebos, H. J., Velzen, V., Bruinsma, N., Jacobsen, N., & Waßmuth, S. (2021). Scaling and performance of a flexible mesh bag scour protection. *Proceedings of the 10th International Conference on Scour and Erosion*, 10.

Roulund, A., Sutherland, J., Todd, D., & Sterner, J. (2016). Parametric equations for shields parameter and wave orbital velocity in combined current and irregular waves. *ICSE 2016 (8th International Conference on Scour and Erosion)*.

Roy, S., Debnath, K., & Mazumder, B. S. (2018). Distribution of turbulent eddies behind a monopile for vortex lock-on condition due to wave current combined flow. *Coastal Engineering*, *131*, 70–87. https://doi.org/10.1016/j.coastaleng.2017.10.010

RVO. (n.d.). Offshore wind energy plans 2030-2050 [Accessed: Friday 23rd August, 2024].

Schendel, A. (2018). *Wave-current-induced scouring processes and protection by widely graded material* [Doctoral dissertation, Gottfried Wilhelm Leibniz Universität]. https://doi.org/10.15488/4453

Schiereck, G. J., & Verhagen, H. J. (2019). *Introduction to bed, bank and shore protection: Revised edition*. Delft Academic Press.

Soulsby, R. (1997). *Dynamics of marine sands*. Thomas Telford Publishing. https://doi.org/10.1680/doms.25844

Sumer, B., & Fredsøe, J. (1997). *Hydrodynamics around cylindrical structures*. World Scientific.

The North Seas Energy Cooperation. (n.d.). Energy [Accessed: Friday 23rd August, 2024].

Topsector Energie Projecten. (n.d.). Prediction of progressive wear in cable protection systems [Accessed: Friday 23rd August, 2024].

Tramontanaengineering. (n.d.). Failure of cable protection systems [Published: March 1, 2021].

Van Gent, M. (1995). Porous flow through rubble-mound material. *Journal of Waterway Port Coastal and Ocean Engineering*, *121*. https://doi.org/10.1061/(ASCE)0733-950X(1995)121:3(176)

Van Rijn, L. (2019). Critical movement of large rocks in currents and waves. *International Journal of Sediment Research*, *34*(4), 387–398. https://doi.org/https://doi.org/10.1016/j.ijsrc.2018.12.005

Vos, L. D., Rouck, J. D., Troch, P., & Frigaard, P. (2011). Empirical design of scour protections around monopile foundations: Part 1: Static approach. *Coastal Engineering*, *58*, 540–553. https://doi.org/10.1016/j.coastaleng.2011.02.001

Wiberg, P. L., & Sherwood, C. R. (2008). Calculating wave-generated bottom orbital velocities from surface-wave parameters [Predictive Modeling in Sediment Transport and Stratigraphy]. *Computers & Geosciences*, *34*(10), 1243–1262. https://doi.org/https://doi.org/10.1016/j.cageo.2008.02.010

Wu, Y., Fan, Z., & Lu, Y. (2003). Bulk and interior packing densities of random close packing of hard spheres. *Journal of Materials Science*, *38*, 2019–2025. https://doi.org/10.1023/A:1023597707363

Zhao, K., Wang, Y., & Liu, P. L.-F. (2024). A guide for selecting periodic water wave theories - le méhauté (1976)'s graph revisited. *Coastal Engineering*, *188*, 104432. https://doi.org/https://doi.org/10.1016/j.coastaleng.2023.104432

A

Scaling

A.1. Rock bag fabrication and overview

There are sewing patterns for making round bags out of flat fabric, but they are time-consuming and difficult to make. Folds in the fabric around the bag are difficult to avoid. So, the bag is made from a flat circular piece of fabric. For each size of bag, the first bag is hand-shaped to the appropriate diameter and height. The amount of fabric required is marked for subsequent bags of the same size. For the shape, avoid tying the bags too tightly because this will distort the shape and cause the bag to be too high. The knot leaves a small protrusion of bag material at the top. This is not taken into account when measuring the height of the bag, so the height is determined by the top of the rocks.

Bag number	Weight [g]	Diameter [mm]	Hieght [mm]	Target height [mm]	d_{50} [mm]	Theoretical porosity [-]	Density [kg/m3]	d50/D [%]
FL1	37.6	60	16	15	1.9	0.4	1500	3.2
FL2	88.8	80	22	20	1.9	0.4	1500	2.4
FL3	75	75	19	17.5	1.9	0.4	1500	2.5
FL4	177.6	100	24	23	1.9	0.4	1500	1.9

Table A.1: Overview of low density fill material bags

Bag number	Weight [g]	Diameter [mm]	Hieght [mm]	d50 [mm]
S31	125.8	75	18	3.1
S32	127.2	75	18	2.36
S33	126.8	75	17.5	2.36
S34	125.8	75	18	2.36
S12	64.4	60	15	1.9
S13	62.4	60	15	1.9
S14	63.4	60	15	1.9
S15	63.8	60	16	1.9

Table A.2: Additional bags used for grouped tests

A.2. Filling material gradings

Overview of graded material used as filling material for the bags.
Prototype and Wide graded filling material. In figure A.1 the minimum material is larger at model scale, because of the requirement that it must be large enough to not fall out of the bag. At prototype some leakage is allowed. To have a wide enough grading the larger material also has to be larger at model scale.
Narrow compared to wide graded filling material in figure A.3.

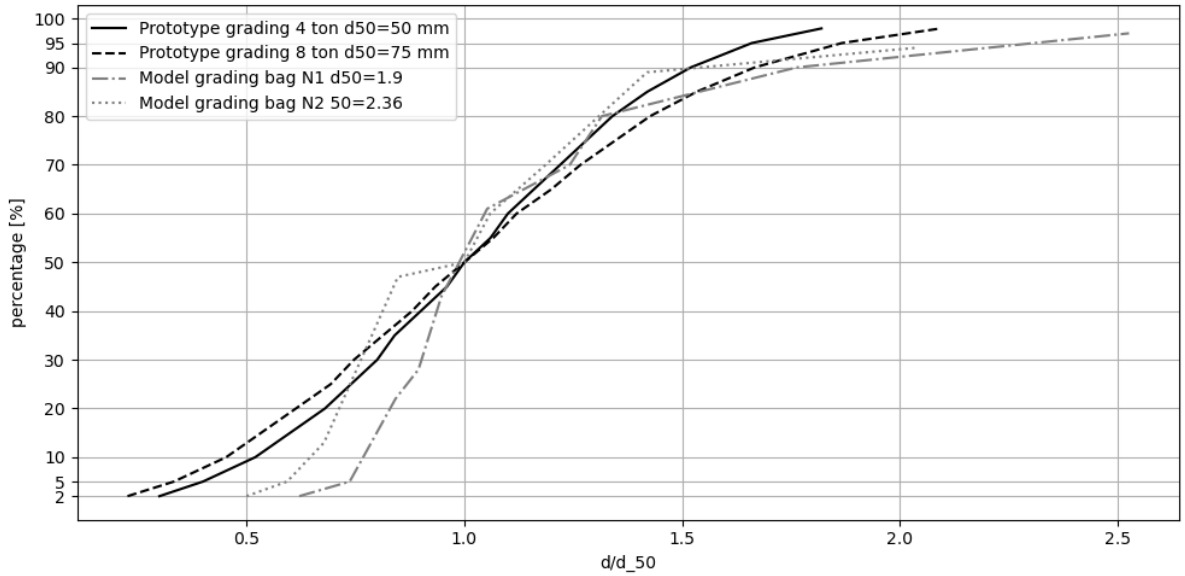

Figure A.1: Normalised prototype and wide graded filling material

Narrow filling material overview in figure A.2.

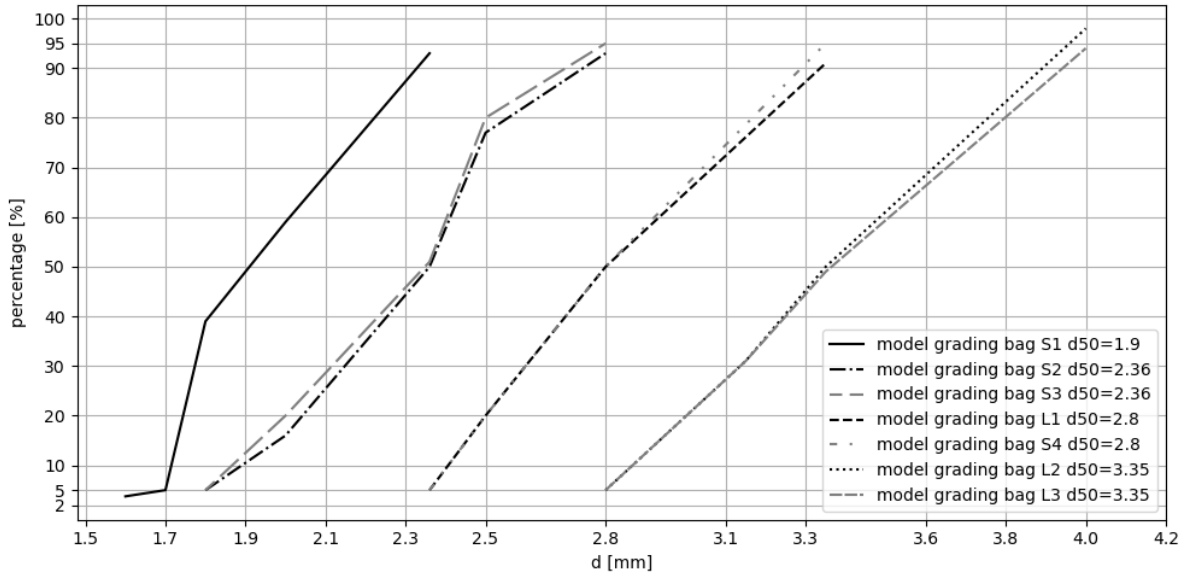

Figure A.2: Overview of narrow graded filling material

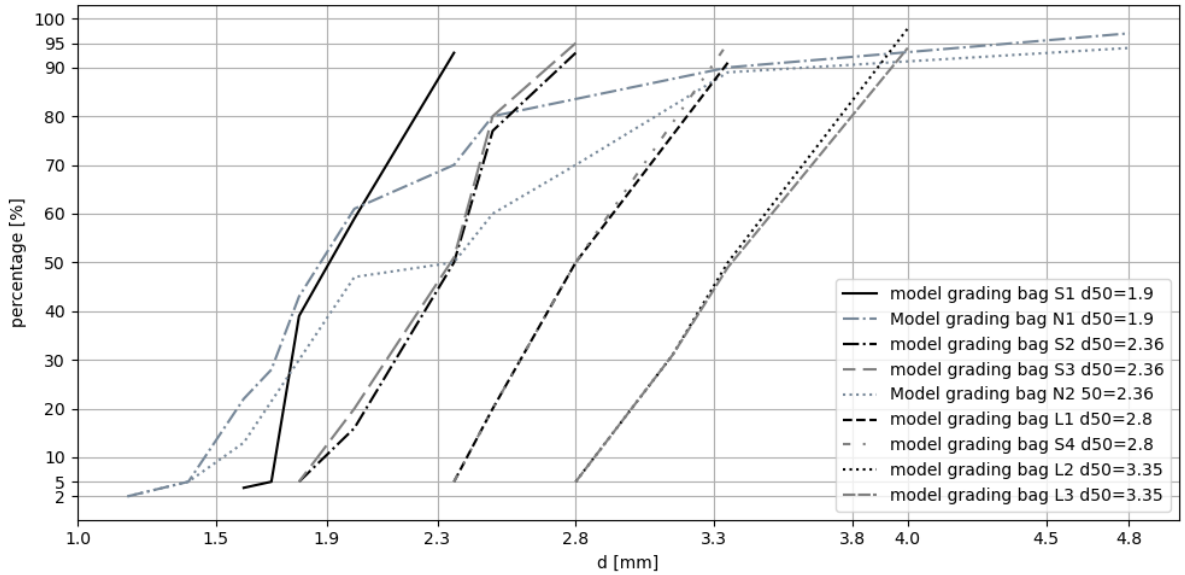

Figure A.3: Comparison of narrow and wide graded filling material

A.3. Hydraulic conditions

Condition	H_{m0} [m]	T_p [s]	u linear $H_{2\%}$ [m/s]	Ursell [-]	Steady current [m/s]	Re steady current monopile $*10^5$ [-]	KC monopile u $H_{2\%}$ [-]
1	0.13	1.8	0.304	9.5	0.14	3.4	2.2
2	0.14	1.8	0.305	10.2	0.14	3.5	2.2
3	0.16	2.1	0.392	16.9	0.14	3.5	3.3
4	0.15	2.1	0.381	30.1	0.15	3.5	4.4
5	0.15	2.2	0.387	26.6	0.14	3.4	4.4
6	0.16	2.2	0.402	31.7	0.14	2.5	4.5
7	0.17	2.5	0.442	34.7	0.14	3.6	5.2
8	0.15	2.8	0.396	54.8	0.14	3.7	7.7
9	0.16	2.8	0.405	36.8	0.10	3.4	5.6
10	0.16	2.9	0.45	15.9	0.14	3.7	3.2
11	0.17	2.9	0.487	52.3	0.14	4.8	6.9
12	0.18	3.3	0.517	17.6	0.14	3.5	3.4
13	0.18	3.4	0.567	18.8	0.15	3.5	3.5
14	0.17	3.4	0.51	57.6	0.19	3.4	7.7
15	0.19	3.4	0.564	51.3	0.14	3.5	6.8

Table A.3: Overview of used irregular wave-current conditions the full model tests. All spectra generated with peak enhancement factor $\gamma = 3.3$, $\sigma_{low} = 0.07$ and $\sigma_{high} = 0.09$.

Condition	H_{m0} [m]	Tp [s]	u linear $H_{2\%}$ [m/s]	Ursell [-]	KC monopile u $H_{2\%}$ [-]
1	0.093	1.4	0.19	2.9	1.0
2	0.15	1.6	0.27	7.0	1.7
3	0.12	1.8	0.33	8.3	2.4
4	0.14	1.8	0.33	9.1	2.4
5	0.15	1.8	0.31	9.7	2.2
6	0.17	1.8	0.34	10.8	2.4
7	0.16	1.8	0.34	11.3	2.5
8	0.17	1.9	0.37	12.1	2.8
9	0.18	1.9	0.37	13.7	2.8
10	0.15	2	0.37	12.6	2.9
11	0.19	2.1	0.45	18.4	3.7
12	0.18	2.2	0.43	20.1	3.7
13	0.19	2.2	0.43	20.2	3.8
14	0.2	2.2	0.46	20.9	4.0
15	0.15	2.3	0.43	18.5	4.0
16	0.2	2.4	0.49	28.1	4.7
17	0.18	2.5	0.46	27.8	4.6
18	0.2	2.5	0.50	29.8	5.0
19	0.13	2.6	0.47	22.8	4.9
20	0.17	2.6	0.45	27.4	4.7
21	0.2	2.6	0.50	32.2	5.2
22	0.17	2.8	0.48	34.2	5.4
23	0.18	2.8	0.45	34.8	5.0
24	0.19	2.8	0.51	35.9	5.7
25	0.2	2.8	0.54	37.8	6.0
26	0.2	2.9	0.51	41.3	6.0
27	0.22	2.9	0.58	44.1	6.8
28	0.15	3.1	0.47	36.8	5.9
29	0.18	3.1	0.59	44.2	7.4
30	0.21	3.4	0.61	60.9	8.3
31	0.18	3.7	0.57	60.8	8.4

Table A.4: Overview of used irregular wave conditions for the full model tests. All spectra generated with peak enhancement factor $\gamma = 3.3$, $\sigma_{low} = 0.07$ and $\sigma_{high} = 0.09$.

B

Analysis of mobility from top pictures

In this appendix a number of figures are shown to provide more insight into the method for determining the classification of test results. In total, 410 comparisons are made of before and after pictures with the method described in the main text. A selection can be seen in the following figures.

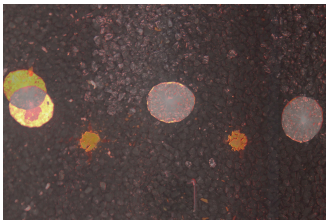

(a) Left bag N1: Failed, right bag S1 and centre L1: Rocking

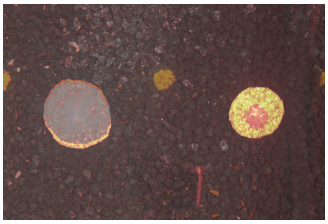

(b) Left bag N2: Rocking, right bag N1: Failed

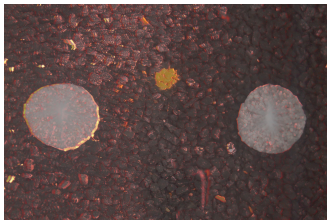

(c) Left bag L2: Rocking, Right bag S2: Stable

Figure B.1: Heat map of difference of before and after picture over the before picture in three regular wave tests.

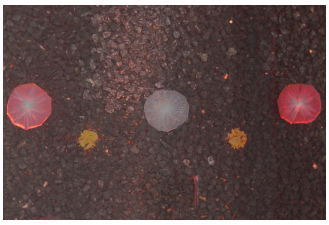

(a) Left bag G3, right bag G1: Rocking and centre bag G1: Stable

(b) Left bag G3: Failed, right bag G1: Failed and centre bag G2: Rocking

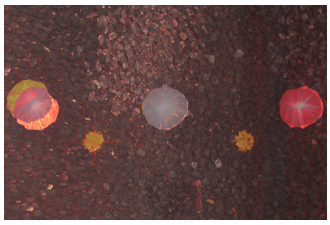

(c) Left bag G3: Failed, right bag G2: Rocking and centre bag G1: Rocking

Figure B.2: Heat map of difference of before and after picture over the before picture in three tests of glass fill material.

(a) Stable

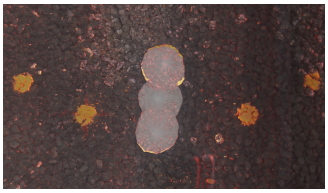

(b) Rocking

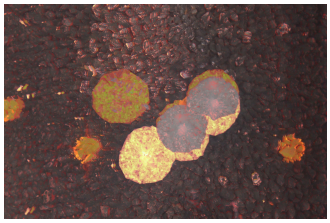

(c) Failed

Figure B.3: Heat map of difference of before and after picture over the before picture in three tests of the 3 bag row formation.

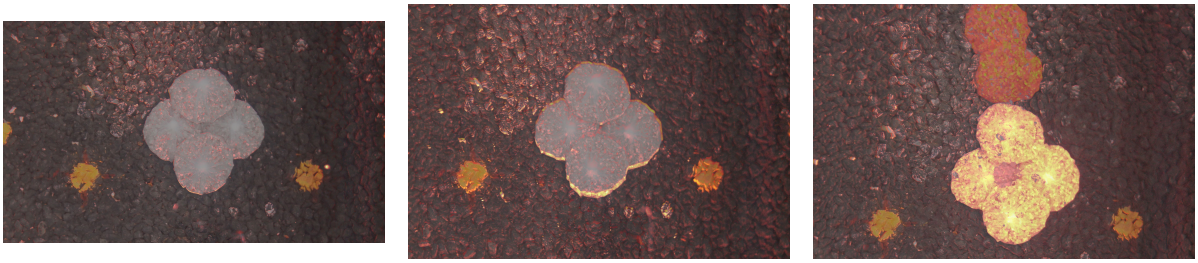

(a) Stable (b) Rocking (c) Failed

Figure B.4: Heat map of difference of before and after picture over the before picture in three tests of the 4 bag diamond formation.

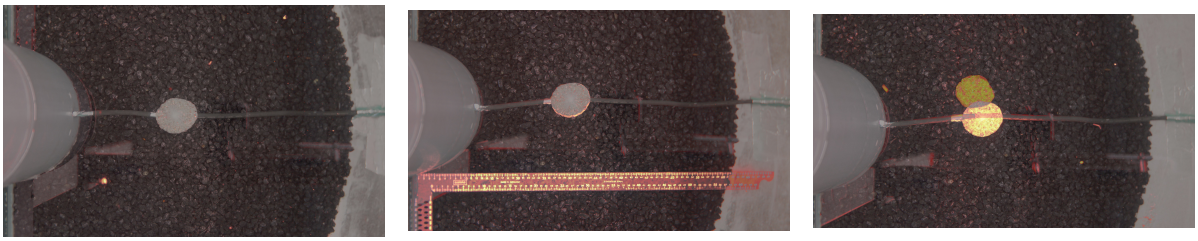

(a) Stable (b) Rocking, ruler in the before picture (c) Failed

Figure B.5: Heat map of difference of before and after picture over the before picture in three tests of a single bag in the full model.

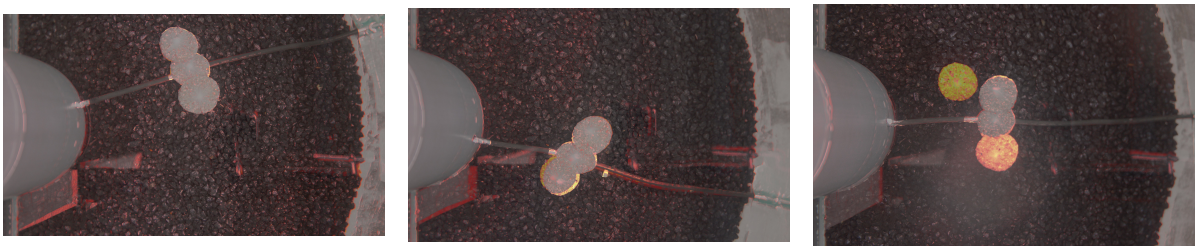

(a) Stable (b) Rocking (c) Failed

Figure B.6: Heat map of difference of before and after picture over the before picture in three tests of the 3 bag row formation in the full model.

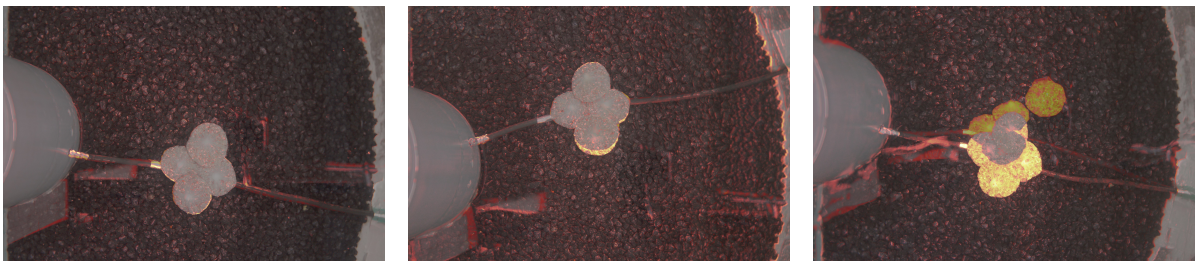

(a) Stable (b) Rocking (c) Failed

Figure B.7: Heat map of difference of before and after picture over the before picture in three tests of the 4 bag diamond formation in the full model.

C

Testing methodology

In this appendix the general approach for the different types of tests is discussed. Table C.1 gives an overview of the different types of tests that were conducted and the general research goal.
The first test conducted were done with bags made to practice the manufacturing process. These were mainly done to try out the wave maker and flume combination, to see if mobility could be reached. The testing procedure was determined and the top camera tested.
In all tests stability was estimated based on the observed motion of the bags during the tests and quick comparison of the top pictures. This method turned out to be reasonably accurate compared to the later analysis of the top pictures.

In all regular wave tests the Jacobsen et al. (2023) limit was used as an indication for the area of interest in the ψ-KC plain. Conditions were designed to obtain a good covering of the plane around the limit. After the first tests with a certain size rock bag more conditions were added in between stable and failure conditions to be able to more precisely find the critical limit. Multiple bags were tested at once side by side, to rule out the location in the array as a factor, bags were swapped multiple times.
For irregular waves there was no information on the expected stability. So, the conditions of multiple wind parks were scaled for as a basis. The wave heights and periods were adapted based on the observations made during the test. If a stable conditions was used to start the wave height and period were increased until failure was reached. The other way around if the series started with failure.
For the tests of grouped formations a number of conditions were repeated for all formations to be able to compare them directly, for both the low density and normal density material.

Test type	Number of tests	Research goal
Start-up tests	15 regular waves, 2 irregular waves	Determine test procedure
Regular waves	138 tests, 288 bags	Stability limit and influence of parameters
Irregular waves	21 tests, 52 bags	Stability limit and influence of parameters
Gain of stability	8 tests, 5 regular waves, 114 data points	Gain of stability effect
Combined wave current	56 regular wave tests, 139 bags	Stability limit and applicability of equation
Glass material	34 regular wave tests, 98 bags	Influence of internal friction
Low density material	29 regular wave tests, 58 bags	Influence of density
Grouped bags	62 regular waves	Performance of grouped bags and formation
Monopile foundation with cable	45 irregular waves, 26 irregular waves with current	Performance of single and grouped bags for CPS stabilisation
Monopile foundation without cable	7 irregular waves, 24 regular waves	Influence of CPS on stability
Conference tests (Low water level)	13 irregular waves with low water level	Performance of single and grouped bags for CPS stabilisation
Total	114 irregular waves, 366 regular wave tests	

Table C.1: Overview of conducted experiments, the number of tests and the research goals for the tests.

C.1. Gain of stability

During testing it was observed that often most movement of the bags is seen during the first waves of a test. The movement subsides during the test and the bags seem to become more stable. Is there a gain of stability effect due to rearrangement of the material in the bag? For all other experiments the bags were lifted between tests to rule out this influence. Some test have done to investigate a possible gain of stability, where a number of regular wave conditions are done with increasing energy to try to observe a gain in stability. Only before and after pictures are taken and the data is difficult to

analyse, as described for the normal regular wave tests, but in these tests the wave fields are difficult to separate. From direct comparison of input wave data the results are inconclusive. So this is not further investigated. A possible gain of stability would be an argument to do further testing with irregular waves. In prototype all conditions are irregular and smaller waves will cause some rearrangement of the fill material.

D

Analysis of wave data

D.1. Regular wave tests

The following section will describe the method for analysing the data from regular wave tests.
Theoretically, in a regular wave field all waves are the same and therefor cause constant orbital velocities. Unfortunately, high reflections during the tests and limits of the wave maker for steep- and highly non-linear waves cause fluctuations in the wave fields. The average reflection coefficient in the regular wave tests was 0.27. Because of the regular wave periods, the interference pattern between the incoming and reflected signal is both space and time dependent. This leads to differences in wave heights and orbital velocities at the locations of the wave height gauges, EMS' and test set-up. In irregular wave fields a Fourier decomposition of the wave signal can be used to split the incoming and reflected signal. For this method to work each harmonic component needs to propagate at the celerity based on the period depended dispersion relation. The highly non-linear waves used for these experiments, are characterised by a combination of bound harmonics, propagating with the same velocity. As a result, Fourier decomposition of the signal coupled with calculation of the celerity of each component based on the dispersion relation does not result in a satisfactory characterisation of the wave field. In order to characterise the wave field and find an expression for the orbital velocities experienced by the rock bags the following method is proposed:
When a wave field is started the wave maker has a number of start up waves before the actual waves of the field. Taking these start up waves of the field into account, for all wave velocities seen during the testing campaign the first four full sized waves at the gauges are free of reflections. These are assumed to be representative for the output of the wave maker and therefor the incoming signal. These waves are averaged for the different wave gauges and combined into a single representative wave. For some wave conditions, there are noticeable differences between those first waves.
The wave signals from the three different gauges are overlaid by taking the time gaps into account based on the distances between the wave gauges and the average recorded zero crossing period. Despite the non-linear wave shapes this gives an accurate result, as is suggested by Fenton (1990) for the case without current. The three signals are subsequently combined into a single average water surface elevation signal.

D.1.1. Reflected signal

To find the reflected signal, the representative wave is subtracted from this combined signal. To take small differences in wave period and possibly propagation speed in to account, this is done for each wave in the signal by matching the first zero-crossings.
For the reflected signal it is assumed that it consists only of free waves, so a Fourier decomposition is possible. From the signal a energy density spectrum is made. This shows multiple distinct narrow peaks. Based on trial and error it turned out that using the three highest peaks for a harmonic representation of the signal gave the best result. Around each peak the energy is summed from 0,95 to 1,05 times the peak frequency. The harmonic representation of the reflected signal is constructed with equation D.1. See Figure D.1.

$$\eta = \sum_{n=1}^{3} 2\sqrt{\int_{0,95f_{p,n}}^{1,05f_{p,n}} E(f)df}\,\sin(\omega_{p,n}(t-\varphi_{p,n}) - kx) \tag{D.1}$$

$$\omega_{p,n} = 2\pi/f_{p,n} \tag{D.2}$$

$$r_{p,n} = a + bi \tag{D.3}$$

$$\varphi_{p,n} = arctan(a/b) \tag{D.4}$$

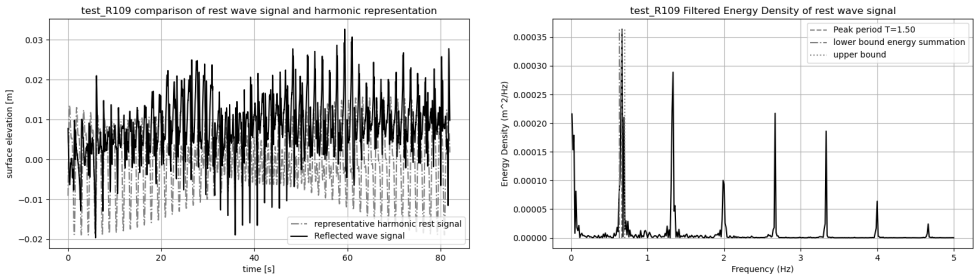

Figure D.1: Reflected signal, energy density of reflected signal and harmonic representation test R109

The average wave is represented as a 5th order Stokes wave using the equations proposed by Fenton (1985), using the algorithm by Ma (2020) for the fit. For regular waves a 0.55 wave height to depth ratio was not exceeded in these experiment, so both Stokes- and Cnoidal wave theories should perform well according to Fenton (1990). In the interest of limiting computation time and complexity the Stokes theory is used. For a few test the fit does not perform well, possibly due to the limits of the wave theory (Zhao et al., 2024). These waves are usually very non-linear or there are lower peaks visible in the wave troughs, due to the formation of spurious waves. Often this fitting problem mostly effects the shape of the trough as the higher order components cause ripples there. The peak height is correct for most waves.

D.1.2. Orbital velocities

From here the orbital velocity at x-locations in the flume can be determined in multiple ways. The first is to only evaluate the orbital velocity of the incoming wave signal using the Fenton (1985) definition. The velocity determined in this way is the fitted wave velocity. If the reflected waves are small this can be a valid strategy because the influence of the reflected orbital velocities near the bed will be minimal. In these experiments the reflected waves do reach sizes where there is an effect on bottom orbital velocity. The median ratio of reflected wave height to the incoming wave height is 27%. To take this into account the combined incoming and linear reflected wave bed orbital velocities are calculated. With the reflected orbital velocity from linear wave theory, as these waves are smaller. Both are corrected for the x-position in the wave flume, since the interference pattern is space and time dependent, using equation D.1.

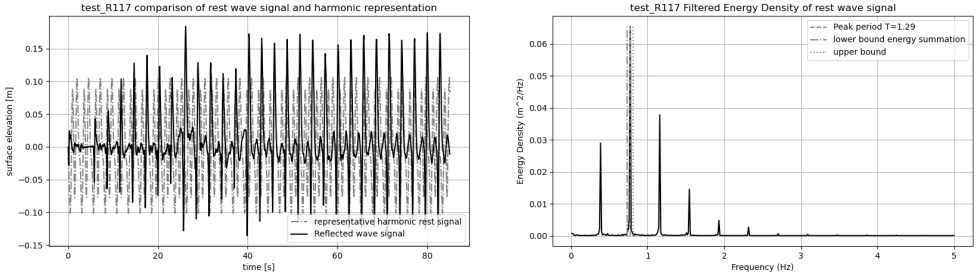

Figure D.2: Reflected signal, energy density of reflected signal and harmonic representation. Test R117: maximum reflected H_{m0}

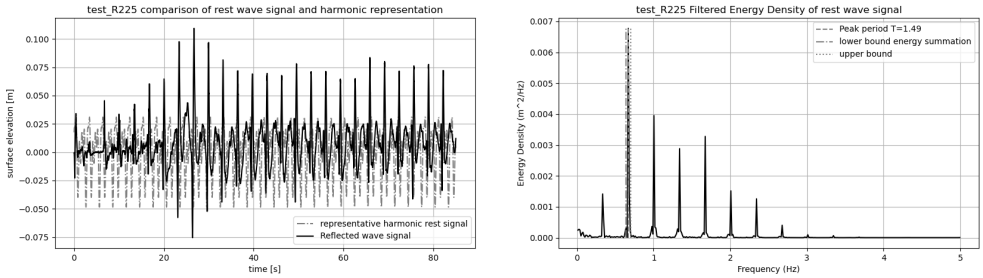

Figure D.3: Reflected signal, energy density of reflected signal and harmonic representation test R225

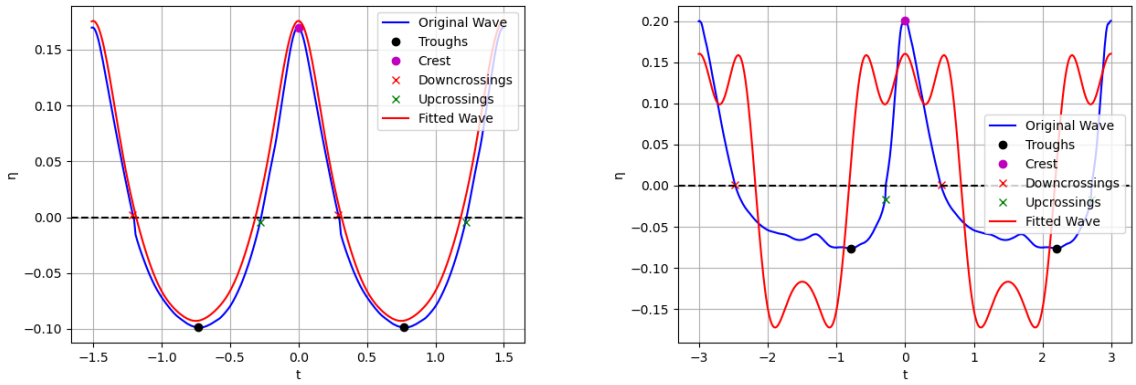

Test R109: good fit

Test R225: bad fit

Figure D.4: Fitted fifth order waves (red) compared to averaged incoming wave signal (blue). Fit made with the method by Ma (2020)

The height used for the computation of orbital velocities at the set-up is assumed 4 cm above bed level for the centre of the rock bags. The EMS' are set at 10 cm above bed level, so theoretical velocities used to for comparison to the EMS data are evaluated at that height.
During the tests the orbital velocities were measured at two locations between the wave height gauges and the set-up. There is reason to distrust the maximum amplitudes of the orbital velocity measurements. As in some tests they are lower than the calculated velocities even during the first few peaks when there are no reflections yet. In other cases there is good correspondence with the fitted wave amplitudes or with the combined wave amplitudes. Or with one of the two, or only with the positive or negative amplitudes. See Figures D.6 to D.9 for examples. The correspondence seems dependent on the interference of incoming and reflected signals. In the irregular wave tests there also is a difference in amplitude between the measured and calculated velocities, see Figure D.13. In Figure D.9 the flat peaks of the measured orbital velocity signal are noticeable.

In 31 tests either the positive or negative peak amplitudes of the combined velocity are exceeded by the average measured velocity amplitude. For 25 tests the combined velocity amplitudes are not exceeded but the fitted wave velocity amplitudes are. For 82 tests the combined velocity and fitted wave velocity amplitudes are not exceeded by the average measured positive or negative velocity amplitude.
The negative velocity estimates seem incorrect in many tests with a high Ursell number. For these tests the fitted wave is not correct in the trough, probably causing this. In Figure D.5 the ratios of positive and negative velocity amplitudes are plotted based on the waves Ursell numbers. Where the measured ratio keeps increasing for higher Ursell numbers, as predicted by theory, the calculated ratios start to decrease. This is due to too large negative amplitudes for the fitted waves. This is caused by the bad fits in the troughs. Cnoidal theory might have resulted in a better fit for these tests.
The Jacobsen et al. (2023) limit is based on second order wave theory orbital velocities. For irregular waves the orbital velocities will be based on linear wave theory calculations, as the shape of waves

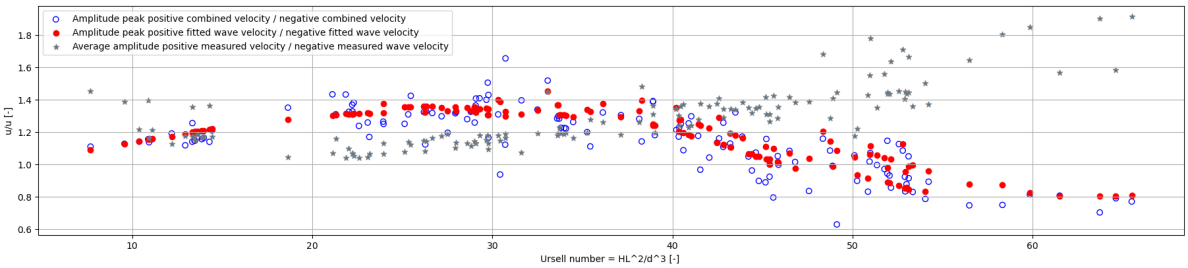

Figure D.5: Comparison of ratios of orbital velocity statistics compared along the Ursell numbers of the tests for regular wave tests. For the higher Ursell number conditions there is a difference in the ratio of positive and negative amplitudes in orbital velocity between the fitted wave (red), combined wave (blue) and measured (grey) orbital velocities. This is likely due to the incorrect wave fit in the troughs, leading to overestimation of the negative component.

that are made up from many components is difficult to predict. For linear waves the ratio between the positive and negative velocity amplitudes is one. This is not the case for the fifth order waves. The decision is made to use the positive velocity amplitude and disregard the untrustworthy negative velocity that comes out of the analysis. Every failing or rocking bag except one is displaced to the side or in the positive direction. So, the positive component is thought to be most critical.

In tests where the maximum positive combined orbital velocity is lower than the positive amplitude of the fitted wave velocity, the latter is chosen for the analysis. The first waves to pass the rock bags are not affected by the reflections and the reflections are not constant as is assumed with the harmonic reconstruction. Thus, in those cases the higher fitted wave velocities are experienced by the bags and might have caused failure. In some tests the combined velocity is extremely high compared to the fitted wave, this is deemed untrustworthy and unlikely to have been the case during the entire test. For most of these conditions the combined velocity is much larger than the measured velocity at the EMS locations. If the combined velocity is larger a maximum increase of 15% above the fitted wave velocity is allowed, else the fitted wave velocity is chosen for analysis. This limit is chosen based on the comparison of orbital velocities at the EMS locations, as in figures D.6 to D.9. This has to be done in order to filter out bad results for the reflected signal. These can cause very high combined velocities, while the bags remained stable. The 15% is arbitraty and seems to filter out most of these untrustworthy velocities. In 34 regular wave tests the used velocity is changed from the combined velocity to the fitted wave velocity. For 59 tests the combined velocity is used and for 42 tests the fitted velocity, as this was larger than the combined. If the maximum allowed increase is raised to 20%, this decreases to 24 tests where the velocity is changed and 69 with the combined velocity. In this case there are multiple tests where the rock bags were stable and the measured velocities are much lower than the combined velocity. These show stable or rocking points with a very high φ in the scatter plot and could be called positive outliers. One such example is test R19, indicated for the fitted wave velocity in Figure 5.6.

Three tests results are excluded as these are deemed too untrustworthy. First test R304, because no wave fit is possible with the used method, for an unknown reason. It is a test of the 1 to 40 wide graded bags, the four ton fails and the eight ton is stable. If the average positive measured velocity by the EMS is used the four ton bag has failed bellow the stability limit. Since these measured velocities are often lower than the calculated ones and in another location, this is not taken into account. In both tests R106 and R206 there is a very strong increase in measured velocities, larger than those indicated by the combined velocities at the EMS locations, this is probably the same at the test-set up. Because, the high uncertainty in these tests they are disregarded. The input waves are near the upper limit for the wave maker and the highest energy waves (very near to the highest ursell numbers) in this testing series (H=33 cm, T=2.6, d=60 cm). All four bags tested fail and three are displaced out of frame of the camera's.

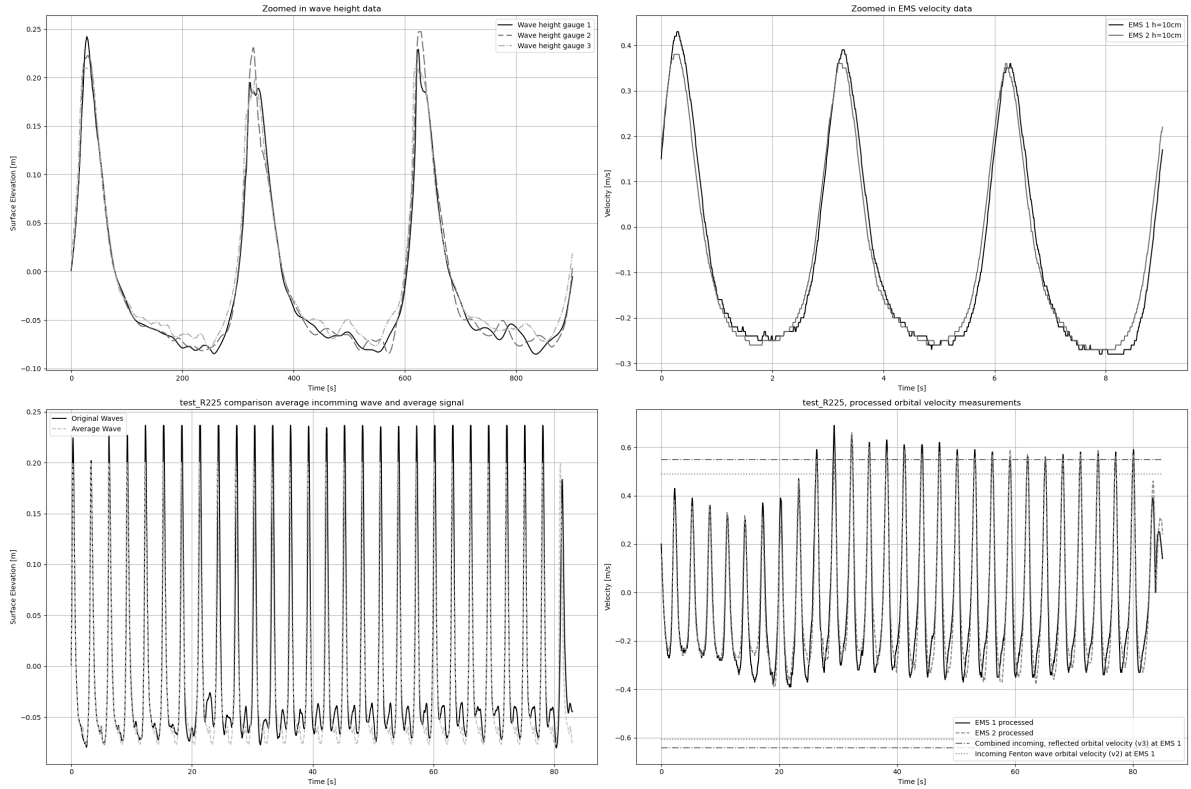

Figure D.6: Test R225: Overview of regular wave test analysis with a bad wave fit.

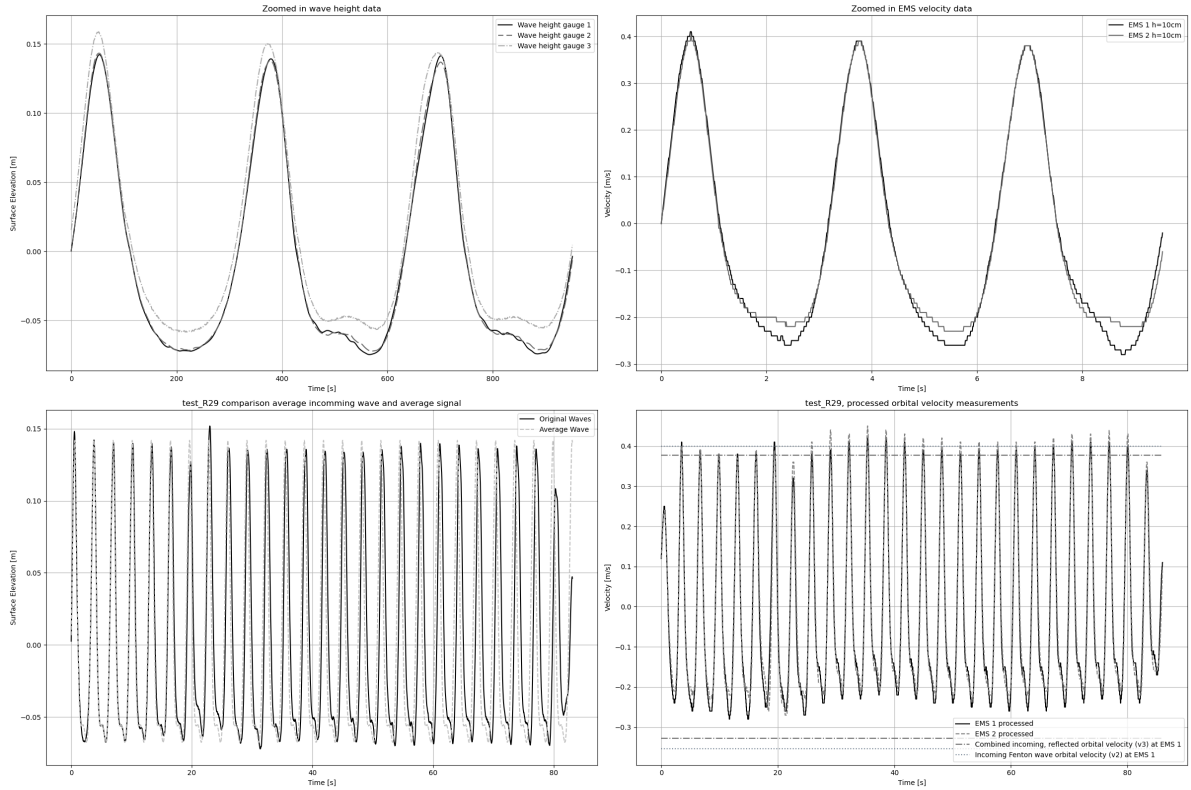

Figure D.7: Test R29: Overview of regular wave test analysis with a bad wave fit.

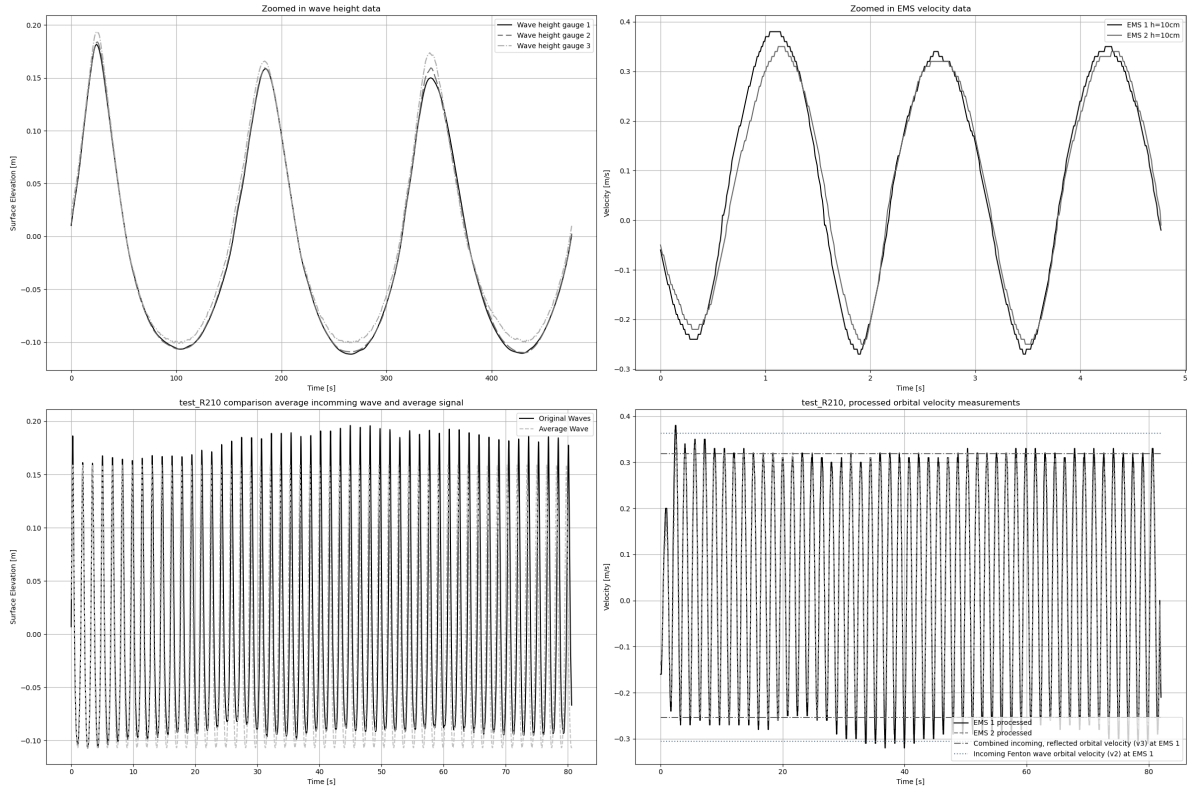

Figure D.8: Test R210: Overview of regular wave test analysis with a good wave fit.

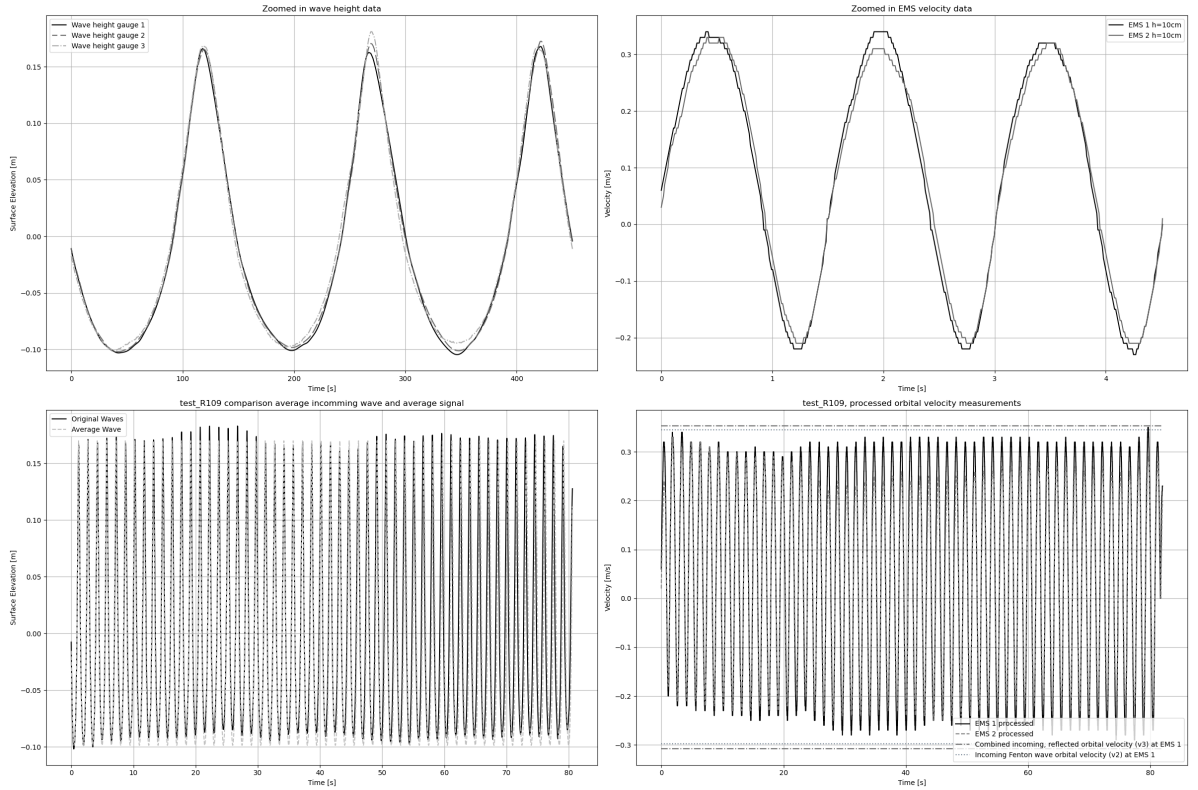

Figure D.9: Test R109: Overview of regular wave test analysis with a good wave fit.

D.2. irregular wave tests

In this section the analysis irregular wave tests are discussed. The wave were measured by a three gauge array and two EMS velocity probes. The wave height data is analysed by spectral decomposition. Incoming and reflected waves are separated. Up to 40% reflection in the larger waves and generally round 20% reflection for the $H_{m,0}$. There mostly constant reflection over the entire spectrum, but relatively large reflections are seen in most test for the component with a period close to 5 seconds, see Figure D.11. In irregular wave fields the interference pattern of incoming and reflected waves is non-correlated in space. So both the incoming and reflected component of the waves is taken into account in further analysis for the orbital velocities.
In many tests the third wave gauge in the array was unable to capture the full amplitude of the highest waves, because the device did not work properly and fails to register waves above a certain level. See Figure D.11, as for wave gauge three the surface elevation does not exceed 0.2 m. In later test the device was raised somewhat to mitigate this issue. When there is a large difference between the wave height statistics from that gauge with the other two it is disregarded and only the average of the first two is used.
The peak period is very close for all gauges and to the average incoming signal period. This was generally a bit larger than the wave maker input, by a few hundredths of a second. Waves are only counted for the Rayleigh wave height distribution when they exceed 5 mm, in order to avoid noise from influencing the exceedance probability distribution. Wave gauge three, or the amplifier it was connected to, had an order of magnitude larger noise level compared to the other gauges.

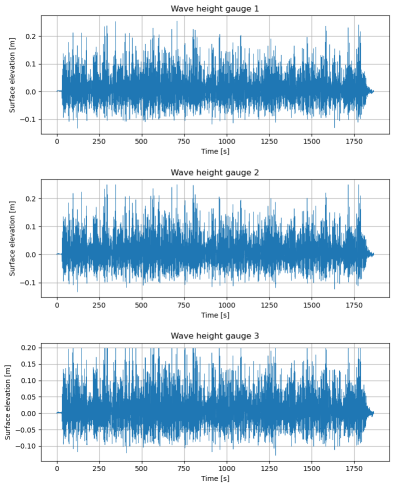

Full wave gauge data from the three wave gauges

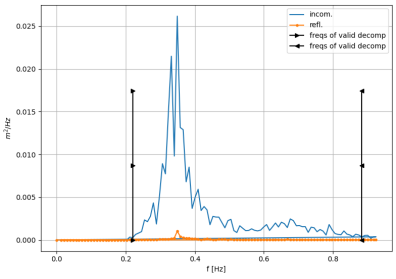

Averaged incoming and reflected spectrum and decomposition range

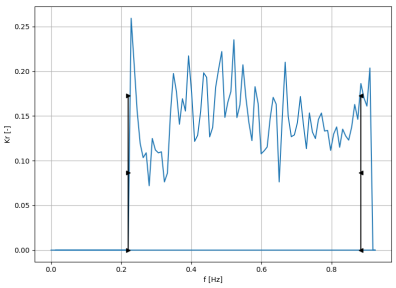

Coefficient of reflection over the decomposition range

Figure D.10: Overview of data for irregular wave test I18

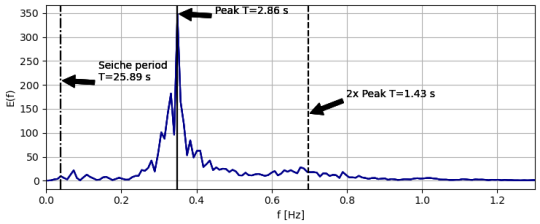

Averaged single sided energy density spectrum

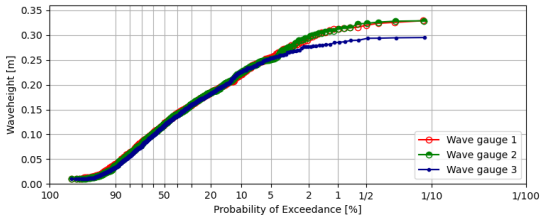

Rayleigh distribution wave heights

Figure D.11: Energy density and wave height distribution of irregular wave test I18

D.2.1. Influence non-linear wave shapes

In table 3.6 the range of Ursell numbers for 50 year design conditions in four wind parks are shown. For the H_{m0} wave these are in the range $14 < Ur_{m0} < 24$. In the irregular wave tests a broad range

of conditions are used in the range $3 < Ur_{m0} < 60$. In Figure D.13 all Ursell numbers of tests can be seen. During the COASTLAB24 conference workshop two tests with an extremely low water level were conducted. These tests have a $Ur_{m0} > 60$, not included in the figure. In an irregular wave field the larger waves have higher Ursell numbers than smaller waves and are thus more non-linear. The use of the values from linear wave theory is assumed to be an reasonable approximation. Non-linear waves have a longer trough period compared to peak period, this raises a question about the meaning of the used parameter $KC = uT/D$ as the full wave period is used there, but the wave velocity signal is characterised by one short duration large amplitude flow and a longer duration flow with lower amplitude.

D.2.2. Measured orbital velocities

Figure D.12 illustrates the processed orbital velocity data from an irregular wave test with the full model. The Rayleigh distribution for positive and negative velocity amplitudes is shown. In this test, the positive and negative amplitude are similar. The two variance spectra differ in terms of their shape and peak frequencies. In the surface elevation variance spectra a peak in variance can be seen near twice the peak frequency. The absence of such a peak is likely due to the orbital velocities of these smaller waves not reaching the level of the EMS'.

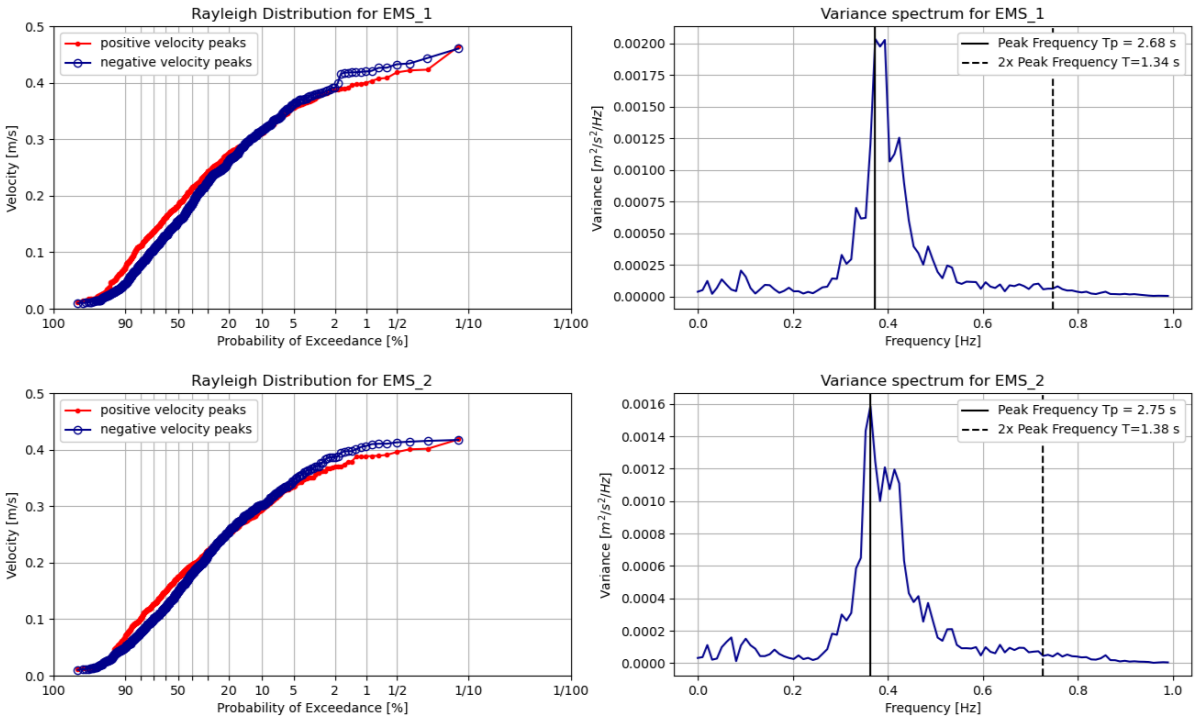

Figure D.12: Rayleigh distribution and variance spectrum for the wave orbital velocity measurements by both EMS' in full model test P21

In Figure D.13 the ratios of multiple velocity measurements and calculated components are plotted against the Ursell numbers of the H_{m0}. Between the calculated velocity of H_{m0} and the measured significant component U_{m0} there is a very consistent difference of approximately 20%. That is: the calculated velocity for the significant wave is on average 122.7% of the measured significant velocity amplitude., with a low spread.

For the 2% calculated and measured values this difference is on average similar, but with a much larger spread, between 100% and 125%. The ratio depends strongly on the Ursell number, with lower differences (100-110)for small Ursell numbers and larger ones for higher Ursell numbers. For Ur>25 the differences are close to ones for the significant value.

This same effect is seen for the negative and positive velocities with the negative ones larger for lower Ursell numbers, but this ratio changes for the larger ones. For non -linear waves a higher positive orbital velocity would be expected, while for linear waves the expected ratio is 1 to 1.

A first explanation could be that the EMS' are not able to capture the peak in orbital velocity. That is why for the m0 components there is a constant offset, as these waves are less non linear compared to the higher exceedance probability waves. For the 2% velocities, the EMS' might capture the negative velocities better because these have a longer period than the positive velocity, even at lower Ursell numbers. With the increasing Ursell number the positive amplitudes increase and the EMS' are able to detect part of this increase, causing the positive amplitudes to overtake the decreasing negative amplitudes. The linear wave theory orbital velocity should be between the positive and negative amplitudes of the non-linear wave, but instead it is often larger than both. In two irregular wave field tests with a monopile the bags fail in the negative direction, but for these tests the ratio of measured positive and negative 2% velocities is close to 1.
Another explanation for the larger negative velocities could be reflections. There is an observed increase in reflections for higher energy waves, that also have a larger Ursell number. However, the interference between the incoming and reflected waves is random and the reflected waves are more linear, because per definition they have smaller Ursell numbers. So reflected waves should not necessarily increase the negative velocities.
In the field, spectral wave height data from measurements or significant wave height and peak periods from a hindcast model are be used to calculate orbital velocities. These are typically in good agreement with measured orbital velocities (Wiberg and Sherwood, 2008).Therefore, in this study, the calculated orbital velocities from surface elevation data will be used to evaluate stability.

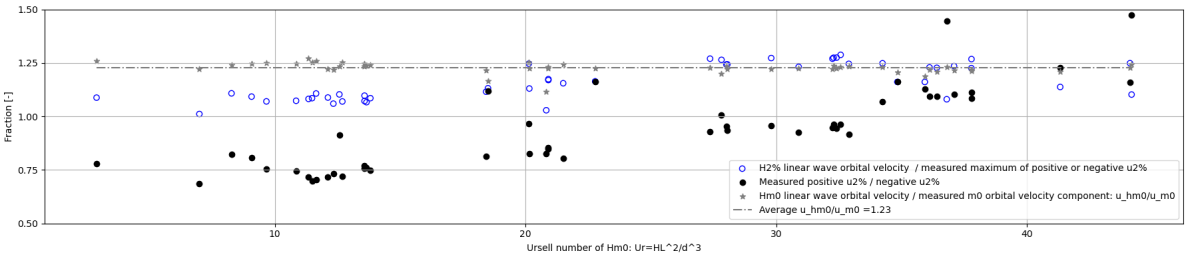

Figure D.13: Ursell sorted tests, with the ratio of the calculated linear velocity caused by the 2% wave to the maximum measured 2% orbital velocity (blue); the ratio of positive/negative measured orbital velocity (black); and the ratio of linear calculated H_{m0} velocity to measured m0 velocity (grey)

D.3. Combined wave-current tests

ARC off in combined current tests, so there might be high reflections. Adapt analysis method to cope with the changed frequency in a fixed point of reference Holthuijsen, 2007:

$$\omega = \sigma + k * U_n \tag{D.5}$$

Absolute frequency is measured by the wave gauges and EMS. To determine the dispersion relation the intrinsic frequency σ is determined. Edited the approximation calculation for the dispersion relation [SFN approximation] with an iterative determination of the wave number with a steady current. A full iterative solution and the Fenton and McKee (1990) approximation to determine the dispersion relation require more computation time. These give the same result for the considered range of periods and currents. The difference with the [SFN approximation] method is $O(10^{-7}$. The same calculation is done for the peak period to determine the wavelength for the Ursell number computation.
Small differences in frequencies EMS and wave gauges. Fixed frame of reference measured frequencies used, as the rock bags are also in a fixed frame of reference. Dispersion calculation for the adapted wave number is only relevant for the determination of the incoming and reflected wave signal. Since for the orbital velocity only the sign matters, there is no need to separate the incoming and reflected signal.
For the computation of the linear orbital velocity the absolute frequency is used, as the rock bags are at a fixed location.
On average the measured steady current is 5% lower in the second EMS compared to the first. This difference is not correlated to the type of wave generated. The difference is likely due to the turbulent flow in the flume not being fully developed near the first EMS. The flow at the set-up will be more developed, but because of the low expected difference this is not taken into account.